ORIGINAL PAPER

Energy-momentum conserving higher-order time integration of nonlinear dynamics of finite elastic fiber-reinforced continua

Norbert Erler[1] · Michael Groß[1]

Abstract Since many years the relevance of fibre-reinforced polymers is steadily increasing in fields of engineering, especially in aircraft and automotive industry. Due to the high strength in fibre direction, but the possibility of lightweight construction, these composites replace more and more traditional materials as metals. Fibre-reinforced polymers are often manufactured from glass or carbon fibres as attachment parts or from steel or nylon cord as force transmission parts. Attachment parts are mostly subjected to small strains, but force transmission parts usually suffer large deformations in at least one direction. Here, a geometrically nonlinear formulation is necessary. Typical examples are helicopter rotor blades, where the fibres have the function to stabilize the structure in order to counteract large centrifugal forces. For long-run analyses of rotor blade deformations, we have to apply numerically stable time integrators for anisotropic materials. This paper presents higher-order accurate and numerically stable time stepping schemes for nonlinear elastic fibre-reinforced continua with anisotropic stress behaviour.

Keywords Galerkin-based time integration · Structure-preservation · Energy-consistency · Finite elasticity · Anisotropy

✉ Michael Groß
  tmd@mb.tu-chemnitz.de; michael.gross@mb.tu-chemnitz.de

[1] Faculty of Mechanical Engineering, Professorship of Applied Mechanics and Dyamics, Technische Universität Chemnitz, Chemnitz, Germany

1 Introduction

This paper is an extension of the works [1] and [2] to a special anisotropic material class, the transversally isotropic material. The base for the investigated time-stepping schemes is the time finite element approach proposed in [3] and [4], in which higher-order accurate time-stepping schemes are developed systematically with the focus on numerical stability in the presence of stiffness combined with large rotations for computing dynamical problems. In the present work, these advantages over conventional time-stepping schemes are combined with highly nonlinear anisotropic material behavior. The presented integrators preserve all first integrals of a free motion of a conservative continuum, i.e. the total linear and the total angular momentum as well as the total energy, which is advantaguous because it guarantees that the discrete configuration vector is embedded in the right solution space [5]. In order to guarantee the preservation of the total energy, the transient approximation of the anisotropic stress tensor has to be enhanced. First, the so-called continuous Galerkin (cG) method in time is used for designing higher-order accurate time integration schemes, which is a common approach (compare [1,6–8] and [9]). In the case of stiff nonlinear elastodynamics, these total energy and momentum conserving time-stepping schemes have better stability properties (see [10] and [11], for instance), which is ideal for medium and long term calculations. Furthermore, the potential of these integrators is demonstrated for example in [12], that includes an enhancement to coupled thermo-mechanical problems.

A common method to enhance the conventional integrators, which is also used in this paper, is to replace an ordinary derivative with a conserving discrete derivative (see, for example, [10,13,14] and [15]). In order to create anisotropic material behaviour, the starting point is the definition of a

free energy density function that depends on a certain strain measure, and additionally on so-called structural tensors (cf. [16–22] and references therein for a detailed discussion), which represent the fibre directions of the fibre reinforced material. In general, polyconvex free energy density functions are well suited for these problems (cf. [23,24] and [18]), and are used in several practical fields of structural mechanics (see, for example, [25,26] and [27]).

In the following, the equations of motion of the generalized problem in Hamitonian formulation are presented. Then, the description of the anisotropic material behaviour based on polyconvex free energy density functions is shown. Subsequently, a finite element discretization in space and time for dynamical problems based on nonlinear anisotropic elastic continua is summarized. Both, conventional momentum-conserving and enhanced energy-momentum conserving time stepping schemes are exhibited, and compared by analysing two representative numerical examples.

2 The dynamical problem in Hamiltonian formulation

The presented time discretization implies a mathematical formulation of the considered dynamical problem with ordinary differential equations of first order. Besides a formulation in the Lagrangian phase space using the generalized velocity vector $\mathbf{v} = \dot{\mathbf{q}}$ as independent variable, there exists the Hamiltonian phase space using the generalized momentum vector $\mathbf{p}$. Since the latter method relates the total linear momentum directly with the time-stepping scheme, the Hamiltonian formulation is advantagous for structure-preserving time-stepping schemes. Note that this advantage is further exploited using variational time integrators (see [28] and references therein), which realise a time-discrete LEGRENDRE transformation, called position-momentum form, making time-stepping schemes momentum conserving, which do usually not conserve momenta as the LOBATTO-quadrature-based trapezoidal rule.

2.1 Equations of motion

In general, semi-discrete nonlinear elastodynamics describe motions of a finite set of material points $\mathscr{B}$, which are placed in the Euclidean space $\mathbb{E}^{n_{\dim}}$, usually modelled by the real coordinate space $\mathbb{R}^{n_{\dim}}$. In a continuous mechanical structure, the material points are finally represented by the spatial finite element nodes.

Let us consider a set $\bar{\mathscr{B}}$ of n_{poi} material points, which are arranged in a configuration $\mathscr{B}_t$ at a given time t. Every material point in this configuration is specified by its position vector $\mathbf{q}^A$ with $A = 1, \ldots, n_{\text{poi}}$. Assuming a free motion of

the mechanical structure, the number of degrees of freedom reads $n_{\text{dof}} = n_{\dim} \cdot n_{\text{poi}}$. The vector $\mathbf{q} = (\mathbf{q}^1, \ldots, \mathbf{q}^{n_{\text{poi}}}) \in \mathbb{R}^{n_{\text{dof}}}$ denotes the coordinate vector of the configuration.

We suppose in this work conservative internal forces due to elastic deformations of a mechanical structure, which is derived from a internal potential energy $V^{\text{int}}(\mathbf{q})$, having the gradient

$$\nabla_{\mathbf{q}} V^{\text{int}}(\mathbf{q}) = \mathbb{Q}(\mathbf{q})\mathbf{q} \tag{1}$$

with a nonlinear symmetric stiffness matrix and a block structure that reads

$$\mathbb{Q}(\mathbf{q}) = \mathbf{Q}(\mathbf{q}) \otimes \mathbf{I}_{n_{\dim}} \tag{2}$$

where

$$\mathbf{Q} = \begin{bmatrix} Q_{11} & \cdots & Q_{1n_{\text{poi}}} \\ \vdots & & \vdots \\ Q_{n_{\text{poi}}1} & \cdots & Q_{n_{\text{poi}}n_{\text{poi}}} \end{bmatrix} \tag{3}$$

Here, the matrix $\mathbf{I}_{n_{\dim}}$ denotes the $n_{\dim} \times n_{\dim}$ identity matrix, and the symbol $\otimes$ designates the direct matrix product.

We refer to the vector $\dot{\mathbf{q}}$ as the velocity vector of the configuration, where the superimposed dot denotes differentiation with respect to time. The kinetic energy T of the configuration is then given as the quadratic form

$$T(\dot{\mathbf{q}}) = \frac{1}{2}\dot{\mathbf{q}}^T \mathbb{M}\dot{\mathbf{q}} \tag{4}$$

with respect to the velocity vector. The non-singular symmetric mass matrix also possesses a block structure that takes the form

$$\mathbb{M} = \mathbf{M} \otimes \mathbf{I}_{n_{\dim}} \tag{5}$$

where

$$\mathbf{M} = \begin{bmatrix} M_{11} & \cdots & M_{1n_{\text{poi}}} \\ \vdots & & \vdots \\ M_{n_{\text{poi}}1} & \cdots & M_{n_{\text{poi}}n_{\text{poi}}} \end{bmatrix} \tag{6}$$

denotes the corresponding structure matrix. Neglecting conservative external forces, the Lagrangian $L(\mathbf{q}, \dot{\mathbf{q}}) = T(\dot{\mathbf{q}}) - V^{\text{int}}(\mathbf{q})$ of this dynamical problem is equal to the difference between the kinetic energy $T(\dot{\mathbf{q}})$ and the internal potential energy $V^{\text{int}}(\mathbf{q})$. The corresponding generalized momentum vector $\mathbf{p} = (\mathbf{p}^1, \ldots, \mathbf{p}^{n_{\text{poi}}}) \in \mathbb{R}^{n_{\text{dof}}}$ of the material points is defined by

$$\mathbf{p} = \nabla_{\dot{\mathbf{q}}} L(\mathbf{q}, \dot{\mathbf{q}}) = \mathbb{M}\dot{\mathbf{q}} \tag{7}$$

The Hamiltonian H follows from the LEGENDRE transformation of the Lagrangian L with respect to the velocity vector as $H(\mathbf{q}, \mathbf{p}) = \mathbf{p} \cdot \dot{\mathbf{q}}(\mathbf{p}) - L(\mathbf{q}, \dot{\mathbf{q}}(\mathbf{p}))$. Hence, replacing $\dot{\mathbf{q}}$ in the Hamiltonian, H is identical with the total energy of the configuration, given by

$$H(\mathbf{q}, \mathbf{p}) = T^*(\mathbf{p}) + V^{\text{int}}(\mathbf{q}) \tag{8}$$

where

$$T^*(\mathbf{p}) = \frac{1}{2}\mathbf{p}^T \mathbb{M}^{-1} \mathbf{p} \tag{9}$$

denotes the conjugate kinetic energy with respect to the generalized momentum vector. The matrix $\mathbb{M}^{-1}$ denotes the inverse mass matrix, which also has a block structure of the form

$$\mathbb{M}^{-1} = \mathbf{M}^{-1} \otimes \mathbf{I}_{n_{\text{dim}}} \tag{10}$$

with

$$\mathbf{M}^{-1} = \begin{bmatrix} M_{11}^{\text{inv}} & \cdots & M_{1n_{\text{poi}}}^{\text{inv}} \\ \vdots & & \vdots \\ M_{n_{\text{poi}}1}^{\text{inv}} & \cdots & M_{n_{\text{poi}}n_{\text{poi}}}^{\text{inv}} \end{bmatrix} \tag{11}$$

where M_{AB}^{inv} symbolize an entry of the inverse mass matrix. Using LAGRANGE-D'ALEMBERT's principle in Hamiltonian form, we find the equations of motion

$$\dot{\mathbf{q}} = \frac{\partial H}{\partial \mathbf{p}} = \mathbb{M}^{-1}\mathbf{p} \tag{12}$$

$$\dot{\mathbf{p}} = -\frac{\partial H}{\partial \mathbf{q}} + \mathbf{f}_{\text{nc}} = -\mathbb{Q}(\mathbf{q})\mathbf{q} + \mathbf{f}_{\text{nc}} \tag{13}$$

in first order form, where the vector $\mathbf{f}_{\text{nc}} = (\mathbf{f}_{\text{nc}}^1, \ldots, \mathbf{f}_{\text{nc}}^{n_{\text{poi}}}) \in \mathbb{R}^{n_{\text{dof}}}$ includes all non-conservative external forces that act on the material points. In this paper, the vector $\mathbf{f}_{\text{nc}}$ includes non-conservative explicitly time-dependent forces.

Combining the generalized coordinates and generalized momenta in the state vector $\mathbf{z} = [\mathbf{q}, \mathbf{p}]^T \in \mathbb{R}^{2n_{\text{dof}}}$, the equations of motion can be written as the following compact system of first order ordinary differential equations:

$$\dot{\mathbf{z}} = \mathbb{J}\nabla_{\mathbf{z}}H(\mathbf{z}) + \mathbf{f}_{\mathbf{z}} \tag{14}$$

where

$$\mathbb{J} = \begin{bmatrix} 0 & 1 \\ -1 & 0 \end{bmatrix} \otimes \mathbf{I}_{n_{\text{dof}}} \quad \text{and} \quad \mathbf{f}_{\mathbf{z}} = \begin{bmatrix} \mathbf{0} \\ \mathbf{f}_{\text{nc}} \end{bmatrix} \in \mathbb{R}^{2n_{\text{dof}}} \tag{15}$$

denotes the symplectic unit matrix and the force vector in the Hamiltonian phase space, respectively.

Remark 1 Considering a continuum body as in this work, the total angular momentum balance principle renders the symmetry of the second PIOLA–KIRCHHOFF stress tensor $\mathbf{S}$ (see [16]). After a spatial finite element discretization as in Sec. 4.1, the total angular momentum balance leads to the symmetry of the matrix $\mathbb{Q}$ in Eq. (1) (see [1]). The symmetry of the second PIOLA–KIRCHHOFF stress tensor also holds for generally composite materials (see [17,18]), in which the fibres are continuously arranged in a matrix material, so that the continuum theory of fiber-reinforced composites can be applied (see Sec. 3.1). Hence, we also obtain for an anisotropic material formulated with structural tensors a symmetric matrix $\mathbb{Q}$ in Eq. (1).

2.2 Energy and momentum conservation

If both the Hamiltonian system does not depend explicitly on time t and is in absence of non-conservative forces, the Hamiltonian $H(\mathbf{q}, \mathbf{p})$ remains constant during the motion. Since for the present problem the total energy and Hamiltonian H is identical, the total energy is conserved inherently (see [2], for more details). Furthermore, it can be shown that both the total linear momentum

$$\mathbf{P} = \sum_{A=1}^{n_{\text{poi}}} \mathbf{p}^A \tag{16}$$

and the total angular momentum

$$\mathbf{L} = \sum_{A=1}^{n_{\text{poi}}} \mathbf{q}^A \times \mathbf{p}^A \tag{17}$$

are also conserved (for a proof may also see [2]).

3 The anisotropic material formulation

Fibre-reinforced polymers are composite materials made of a polymer matrix reinforced with fibres of a different material. These polymers may be modelled for finite strains by an isotropic material law for the matrix, and structural tensors for the fibres (see [29] and [30], for instance). The finite strain model of such an anisotropic elastic material behaviour is introduced in this section.

3.1 Invariant formulation of the free energy

Let $\mathbf{X} \in \mathbb{R}^{n_{\text{dim}}}$ be the coordinates of an arbitrary material point of a solid continuum body $\mathscr{B}$ in the initial configuration $\mathscr{B}_0$ at time $t = 0$. Furthermore, let $\mathbf{x} \in \mathbb{R}^{n_{\text{dim}}}$ be the coordinates of the same material point at any time $t > 0$ in the current configuration $\mathscr{B}_t$, which are defined by the

vector-valued deformation mapping

$$\mathbf{x}(t) = \varphi(\mathbf{X}, t) \tag{18}$$

The deformation directions in the solid continuum are given by the deformation gradient

$$\mathbf{F}(\mathbf{X}, t) = \nabla_{\mathbf{X}} \varphi(\mathbf{X}, t) \tag{19}$$

The right CAUCHY–GREEN tensor as deformation measure with respect to the material configuration $\mathscr{B}_0$ then reads

$$\mathbf{C} = \mathbf{F}^T \mathbf{F} \tag{20}$$

To build an anisotropic material law, we first define a scalar-valued free energy density function (see [31]), which can be a sum of an arbitrary number of free energy density functions that depend on the scalar-valued invariants of the right CAUCHY–GREEN tensor. In general, let all free energy density functions fulfil the requirement of polyconvexity in the sense of Ball [23] to guarantee the existence of minimizers. The main invariants of the right CAUCHY–GREEN tensor read

$$I_1(\mathbf{C}) = \text{tr}(\mathbf{C}) = \mathbf{C} : \mathbf{I} \tag{21}$$

$$I_2(\mathbf{C}) = \frac{1}{2}[(\mathbf{C} : \mathbf{I})^2 - \mathbf{C} : \mathbf{C}] \tag{22}$$

$$I_3(\mathbf{C}) = \det(\mathbf{C}) \tag{23}$$

where the double dot symbol denotes the scalar product of two second-order tensors.

To define the fibre direction of the fibre-reinforced structure, we use so-called structural tensors (see [16,17] and [18], for instance). These are built by a normalized directional vector $\mathbf{a} \in \mathbb{R}^{n_{\dim}}$, which lies in the direction of the fibres in the undeformed reference configuration. The considered structural tensor reads

$$\mathbf{A} = \mathbf{a} \otimes \mathbf{a} \rightarrow |\mathbf{a}| = 1 \tag{24}$$

In general, one can define an arbitrary number of different fibre families by its corresponding directional vectors. In our case, we consider one family of fibres, so we have a special case of anisotropy on hand, the so-called transverse isotropy. Hence, two additional pseudo-invariants of the right CAUCHY–GREEN tensor can be defined as

$$I_4(\mathbf{C}, \mathbf{A}) = \mathbf{C} : \mathbf{A} \tag{25}$$

$$I_5(\mathbf{C}, \mathbf{A}) = \mathbf{C}^2 : \mathbf{A} \tag{26}$$

where the tensor $\mathbf{C}^2$ is equal to the single dot product of $\mathbf{C}$ with itself. These pseudo-invariants describe the stretch of the fibres and the intercation with the matrix, respectively.

3.2 Isotropic free energy

Considering the isotropic part of the free energy density function, it is advantageous to split off the volumetric part $\tilde{\mathbf{C}}$ of the right CAUCHY–GREEN tensor, which only depends on the distortion, but not on the volume change of a volume element of the continuum body. It reads

$$\tilde{\mathbf{C}} = I_3^{-\frac{1}{3}} \mathbf{C} \tag{27}$$

with $\det(\tilde{\mathbf{C}}) = 1$. From this follow the modified main invariants

$$\tilde{I}_1(\tilde{\mathbf{C}}) = \text{tr}(\tilde{\mathbf{C}}) = I_3^{-\frac{1}{3}} I_1 \tag{28}$$

$$\tilde{I}_2(\tilde{\mathbf{C}}) = \frac{1}{2}[(\tilde{\mathbf{C}} : \mathbf{I})^2 - \tilde{\mathbf{C}} : \tilde{\mathbf{C}}] = I_3^{-\frac{2}{3}} I_2 \tag{29}$$

that also depend only on the distortion.

The whole isotropic part of the free energy then is subdivided into an isochoric, i.e. volume-preserving part, and a purely volumetric part in the following way:

$$W^{\text{isotr}} = W_{\text{iso}}^{\text{isotr}}(\tilde{I}_1, \tilde{I}_2) + W_{\text{vol}}^{\text{isotr}}(I_3) \tag{30}$$

with $\tilde{I}_1 = I_3^{-\frac{1}{3}} I_1$ and $\tilde{I}_2 = I_3^{-\frac{2}{3}} I_2$.

3.3 Anisotropic free energy

For the anisotropic part, we also use the modified pseudo-invariants, which read here

$$\tilde{I}_4(\tilde{\mathbf{C}}, \mathbf{A}) = \tilde{\mathbf{C}} : \mathbf{A} = I_3^{-\frac{1}{3}} I_4 \tag{31}$$

$$\tilde{I}_5(\tilde{\mathbf{C}}, \mathbf{A}) = \tilde{\mathbf{C}}^2 : \mathbf{A} = I_3^{-\frac{2}{3}} I_5 \tag{32}$$

Assuming that mechanical energy is only stored due to the distortion of the fibres (but not due to its volume change), the whole anisotropic part of the free energy density function is equal to its isochoric sub-part:

$$W^{\text{aniso}} = W_{\text{iso}}^{\text{aniso}}(\tilde{I}_4, \tilde{I}_5) \tag{33}$$

with $\tilde{I}_4 = I_3^{-\frac{1}{3}} I_4$ and $\tilde{I}_5 = I_3^{-\frac{2}{3}} I_5$.

3.4 Total free energy density function

Since it is assumed that the matrix and the fibre material of the continuum body store the mechanical energy without interaction, the total free energy density function is the sum

$$W = W^{\text{isotr}} + W^{\text{aniso}}$$

$$= W[I_1(\mathbf{C}), I_2(\mathbf{C}), I_3(\mathbf{C}), I_4(\mathbf{C}, \mathbf{A}), I_5(\mathbf{C}, \mathbf{A})] \tag{34}$$

of both the isotropic matrix and the anisotropic fibres. During the practical use in numerical simulations, the total free energy density function should be formulated according to Eq. (34) as functions of the invariants $I_1, \ldots, I_5$, because this represents the universal case that can be handled best to calculate the stress tensor and the corresponding tangent operator (see Appendixes 1 and 5).

4 Time integration of semi-discrete elastodynamics

Considering a continuum body, we have to introduce a spatial discretization to obtain a dynamical system of a finite number of degrees of freedom. In this paper, we apply a BUBNOV–GALERKIN finite element method with linear brick elements as used in Reference [2], in order to allow a comparison of the behaviour of the time integration schemes proposed in this work with the behaviour reported in Reference [2]. But the use of mixed formulations as in Reference [29] using at least Q1/P0 brick elements is to be recommended and realized in the follow-up work. As in Reference [2], the time discretization is performed by a PETROV-GALERKIN finite element method in time called cG method, in contrast to the usually applied finite difference method.

4.1 Finite element discretization in space

In order to clarify the used notation, we summarize the standard spatial finite element discretization of a solid continuum body (see Reference [32], for instance), embedded in a $n_{\dim}$-dimensional Euclidean space $\mathbb{E}^{n_{\dim}}$, and modelled by the real coordinate space $\mathbb{R}^{n_{\dim}}$. In this way, a solid continuum body $\mathscr{B} \subset \mathbb{R}^{n_{\dim}}$ is partitioned into non-overlapping finite elements $\mathscr{B}_e$, $e = 1, \ldots, n_{\mathrm{el}}$. The positions of the element nodes in the initial configuration $\mathscr{B}_0^e$ at time $t = 0$ are denoted by $\mathbf{X}_e^a \in \bar{\mathscr{B}}_0^e$, $a = 1, \ldots, n_{\mathrm{en}}$, and their positions in the current configuration $\mathscr{B}_t^e$ at time $t \in I = [0, T]$ are denoted by $\mathbf{x}_e^a = \mathbf{q}_e^a(t) \in \bar{\mathscr{B}}_t^e$, with the time-dependent position vector $\mathbf{q}_e^a : I \to \mathbb{R}^{n_{\dim}}$ of the node a in the element $\mathscr{B}_t^e$. The arbitrary position $\mathbf{X}_e \in \mathscr{B}_0^e$ and its position $\mathbf{x}_e \in \mathscr{B}_t^e$ are parameterized by the mappings

$$\mathbf{X}_e = \mathbf{\Psi}_e(\eta_e) = \sum_{a=1}^{n_{\mathrm{en}}} N_a(\eta_e) \mathbf{X}_e^a \tag{35}$$

$$\mathbf{x}_e = \mathbf{\psi}_e(\eta_e, t) = \sum_{a=1}^{n_{\mathrm{en}}} N_a(\eta_e) \mathbf{q}_e^a(t) \tag{36}$$

where $N_a : \square \to \mathbb{R}^{n_{\dim}}$, $a = 1, \ldots, n_{\mathrm{en}}$, denote Lagrangian shape functions which satisfy the aimed interpolation condition $N_a(\eta_e^b) = \delta_a^b$, where $\eta_e^b \in \bar{\square}$, $b = 1, \ldots, n_{\mathrm{en}}$, are the element nodes of the e-th element in the parent domain. Further, the material motion $\mathbf{x}_e(\mathbf{X}_e, t) = \psi_e \circ (\mathbf{\Psi}_e)^{-1}(\mathbf{X}_e)(t)$ is

approximated by the deformation mapping

$$\varphi_e(\mathbf{X}_e, t) = \sum_{a=1}^{n_{en}} N_a(\eta_e(\mathbf{X}_e)) \mathbf{q}_e^a(t) \tag{37}$$

The Lagrangian velocity field $\mathbf{v}_e(\mathbf{X}_e, t)$ tangent to the element $\mathscr{B}_t^e$ in the point $\mathbf{x}_e$ is given by $\mathbf{v}_e(\mathbf{X}_e, t) = \partial \varphi_e(\mathbf{X}_e, t)/\partial t$. Further, the spatial tangent attached at the point $\mathbf{X}_e$ in the element $\mathscr{B}_0^e$ arises from the deformation gradient $\mathbf{F}_e = \nabla_{\mathbf{X}_e} \varphi_e$ in the e-th element. From the deformation gradient, the right CAUCHY–GREEN-tensor $\mathbf{C}_e = \mathbf{F}_e^T \mathbf{F}_e$ as deformation measure in the e-th element is derived (see Reference [1] for their explicit expressions). The potential energy V^{int} of the configuration $\mathscr{B}_0$ results from summing over the strain energies

$$V_e^{\mathrm{int}} = \int_{\mathscr{B}_0^e} W_e(\mathbf{C}_e, \mathbf{A}) \mathrm{d}V \tag{38}$$

of the elements. The gradient $\nabla_{\mathbf{q}} V$ of the strain energy then takes the form of Eq. (1), where

$$\mathbb{Q} = \mathop{\mathbf{A}}_{e=1}^{n_{\mathrm{el}}} \hat{\mathbb{Q}}_e(\mathbf{C}_e, \mathbf{A}) \tag{39}$$

follows from assembling the element matrices

$$\hat{\mathbb{Q}}_e(\mathbf{C}_e, \mathbf{A}) = \begin{bmatrix} \hat{Q}_{11}^e & \cdots & \hat{Q}_{1n_{\mathrm{en}}}^e \\ \vdots & & \vdots \\ \hat{Q}_{n_{\mathrm{en}}1}^e & \cdots & \hat{Q}_{n_{\mathrm{en}}n_{\mathrm{en}}}^e \end{bmatrix} \otimes \mathbf{I}_{n_{\dim}} \tag{40}$$

where

$$\hat{Q}_{ab}^e(\mathbf{C}_e, \mathbf{A}) = \int_{\mathscr{B}_0^e} \mathbf{S}_e(\mathbf{C}_e, \mathbf{A}) : \mathbf{N}_{ab}^e \mathrm{d}V \tag{41}$$

includes the material part of the internal force vector components, based on the tensor

$$\mathbf{N}_e^{ab} = \mathbf{J}_e^{-T} \cdot [\nabla_\eta N_a \otimes \nabla_\eta N_b] \cdot \mathbf{J}_e^{-1} \tag{42}$$

denoting the spatial structure matrix of the linearised strain operator $\mathbf{B}_e^a$ with respect to $\mathscr{B}_0^e$. The total kinetic energy T of the initial configuration $\mathscr{B}_0$ is defined as the sum of all kinetic element energies

$$T_e = \frac{1}{2} \int_{\mathscr{B}_0^e} \rho_0 \mathbf{v}_e \cdot \mathbf{v}_e \, \mathrm{d}V \tag{43}$$

$$= \frac{1}{2} \sum_{a,b=1}^{n_{\mathrm{en}}} M_{ab}^e \dot{\mathbf{q}}_e^a \cdot \dot{\mathbf{q}}_e^b \equiv \frac{1}{2} \dot{\mathbf{q}}_e^T \mathbb{M}_e \dot{\mathbf{q}}_e \tag{44}$$

that corresponds with the element cooordinate vector $\mathbf{q}_e = (\mathbf{q}_e^1, \ldots, \mathbf{q}_e^{n_{en}})$. The element mass matrices $\mathbb{M}_e$ have a block structure of the form

$$\mathbb{M}_e = \begin{bmatrix} M_{11}^e & \cdots & M_{1n_{en}}^e \\ \vdots & & \vdots \\ M_{n_{en}1}^e & \cdots & M_{n_{en}n_{en}}^e \end{bmatrix} \otimes \mathbf{I}_{n_{dim}} \tag{45}$$

where

$$M_{ab}^e = \int_{\mathscr{B}_0^e} \rho_0 N_a N_b \, \mathrm{d}V \tag{46}$$

denotes the mass matrix entries. The element mass matrices are also assembled to the global consistent mass matrix $\mathbb{M}$. such that the kinetic energy T and the linear momentum vector $\mathbf{p}$ of the configuration are given by the Eqs. (4) and (7), respectively.

4.1.1 Algorithmic momentum conservation

As it is shown in [2], this spatial discretization on hand preserves the total linear momentum $\mathbf{P}$ and the total angular momentum $\mathbf{L}$, which means that it does not influence both total momenta by the spatial discretization. Keeping both total momenta constant during the whole simulation requires both an unsupported mechanical structure (e.g. the free flight of a blade in Sect. 5) in the absence of external forces.

4.2 GALERKIN-based finite element discretization in time

The considered time interval $\mathscr{T} = [t_0, T]$ of interest is divided into $N_\tau - 1$ non-overlapping subintervals $\mathscr{T}_n$ of length h_n, $n = 1, \ldots, N_\tau - 1$, such that

$$\mathscr{T} = \bigcup_{n=1}^{N_\tau-1} \mathscr{T}_n \tag{47}$$

The partition of the interval T is related with a mesh of time points $t_0 < t_1 < \ldots < t_n = T$. Each subinterval $\mathscr{T}_n = [t_{n-1}, t_n]$ is transformed to a master element $\mathscr{I}_\alpha = [0, 1]$ with respect to the normed time α using the transformation rule

$$\alpha(t) = \frac{t - t_{n-1}}{h_n} \tag{48}$$

where $h_n = t_n - t_{n-1}$ denotes the time step size. Accordingly, the motion in each subinterval $\mathscr{T}_n$ is determined by the following initial value problem with respect to the master element: Given the initial value $\mathbf{z}_0 = \mathbf{z}(t_{n-1})$, find the motion

$\zeta_0 : \mathscr{I}_\alpha \times \mathbb{R}^{2n_{dof}} \ni (\alpha, \mathbf{z}_0) \mapsto \mathbf{z}(\alpha) \in \mathbb{R}^{2n_{dof}}$ determined by the ordinary differential equation

$$\frac{\mathrm{d}\mathbf{z}}{\mathrm{d}\alpha} = h_n \mathbb{J}\nabla_{\mathbf{z}} H[\mathbf{z}(\alpha)] + \mathbf{f}_{\mathbf{z}}(\alpha) \tag{49}$$

with respect to the time $\alpha \in \mathscr{I}_\alpha$. GALERKIN's method determines nodal values of the trial function such that the residual error of the considered differential equation is orthogonal to all functions in the test space. The residual error of the differential equation (49) reads

$$\mathbf{R}(\mathbf{z}) = \frac{\mathrm{d}\mathbf{z}}{\mathrm{d}\alpha} - [h_n \mathbb{J}\nabla_{\mathbf{z}} H(\mathbf{z}) + \mathbf{f}_{\mathbf{z}}] \tag{50}$$

The continuous GALERKIN (cG) method is based on specific polynomials $\mathbf{z}(\alpha)$ of degree k as trial functions and $\delta\mathbf{z}(\alpha)$ of degree $k - 1$ as test functions, which have the form

$$\mathbf{z}(\alpha) = \sum_{J=1}^{k+1} M_J(\alpha)\mathbf{z}_J \tag{51}$$

and

$$\delta\mathbf{z}(\alpha) = \sum_{I=1}^{k} \tilde{M}_I(\alpha)\delta\mathbf{z}_I \tag{52}$$

respectively. Here, $\mathbf{z}_J$ and $\delta\mathbf{z}_I$ denote the corresponding nodal values at equidistant time nodes. The functions M_J and $\tilde{M}_I$ denote LAGRANGE polynomials of degree k and $k - 1$, respectively, with respect to the corresponding equidistant nodes on the master element. A continuous solution is provided by $\mathbf{z}_1 = \mathbf{z}_0$, i.e. for every time step, the first nodal values of the trial functions are given by the final values of the previous time step or, at the beginning of the time interval T, by the initial values of the motion. Then, GALERKIN's orthogonality condition for the residual error $\mathbf{R}(\mathbf{z})$ on the master element $\mathscr{I}_\alpha$ is the weak form

$$\int_0^1 \mathbb{J}\delta\mathbf{z}(\alpha) \cdot \mathbf{R}[\mathbf{z}(\alpha)]\mathrm{d}\alpha = 0 \tag{53}$$

Owing to the fundamental theorem of variational calculus, the weak form in Eq. (53) leads to k vector equations for the k unknown nodal values $\mathbf{z}_J$, $J = 2, \ldots, k + 1$, given by

$$\sum_{J=1}^{k+1} \int_0^1 \tilde{M}_I M_J' \, \mathrm{d}\alpha \, \mathbf{z}_J$$
$$- h_n \int_0^1 \tilde{M}_I \left(\mathbb{J}\nabla_{\mathbf{z}} H[\mathbf{z}(\alpha)] + \mathbf{f}_{\mathbf{z}}\right)\mathrm{d}\alpha = \mathbf{0} \tag{54}$$

with $I = 1, \ldots, k$, where the equations can be divided into two integral terms. The prime denotes here the time derivative with respect to α.

4.3 The continuous GALERKIN (cG) time stepping scheme

Using the gradient of the Hamiltonian H and taking Eq. (15) into account, one finds the following time discretization of the semi-discrete equations of motion, which is called cG(k) method:

$$\sum_{J=1}^{k+1} \int_0^1 \tilde{M}_I M_J' \, d\alpha \, \mathbf{q}_J - h_n \int_0^1 \tilde{M}_I \mathbb{M}^{-1} \mathbf{p} \, d\alpha = \mathbf{0} \qquad (55)$$

$$\sum_{J=1}^{k+1} \int_0^1 \tilde{M}_I M_J' \, d\alpha \, \mathbf{p}_J + h_n \int_0^1 \tilde{M}_I \left(\mathbb{Q}^h \mathbf{q} - \mathbf{f}_{\mathrm{nc}} \right) d\alpha = \mathbf{0} \quad (56)$$

with $I = 1, ..., k$. Generally, the second integral of Eq. (56) has to be determined by numerical quadrature, because its integrand posesses a nonlinearity, caused by the definition of the entries of the approximated stiffness matrix $\mathbb{Q}^h$. This integral is approximated by the k-point Gaussian quadrature rules, because the collocation property of the time stepping schemes has to be taken into account to preserve first integrals, i.e. the total momenta are conserved and the equations of motion are fulfilled exactly at the GAUSS-points ξ_l. A proof may be found in [2]. The quadrature reads

$$\int_0^1 \tilde{M}_I \left(\mathbb{Q}^h \mathbf{q} - \mathbf{f}_{\mathrm{nc}} \right) d\alpha$$

$$\approx \sum_{l=1}^k \tilde{M}_I(\xi_l) \left[\mathbb{Q}^h(\xi_l) \mathbf{q}(\xi_l) - \mathbf{f}_{\mathrm{nc}}(\xi_l) \right] w_l \qquad (57)$$

All other integrals in the Eqs. (55) and (56) can be determined exactly by the k-point Gaussian quadrature rules, because they only include polynomials of degree $2k - 1$.

The time approximation $\mathbb{Q}^h(\alpha)$ of the global stiffness matrix is given by the element stiffness matrices $\hat{\mathbb{Q}}_e^h(\mathbf{C}_e^h(\alpha))$, where $\mathbf{C}_e^h : \mathscr{I}_\alpha \to \mathbb{R}^{n_{\dim} \times n_{\dim}}$ denotes, in general, an arbitrary consistent time approximation of the right CAUCHY–GREEN tensor in the e-th element. The usual cG approximation of the element deformation gradient $\mathbf{F}_e$ is defined by

$$\mathbf{F}_e = \sum_{I=1}^{k+1} M_I(\alpha) \mathbf{F}_I^e \qquad (58)$$

which arise straightforward from Eqs. (19) and (51). The standard time approximation of the right CAUCHY–GREEN tensor then reads $\mathbf{C}_e = \mathbf{F}_e^T \mathbf{F}_e$ according to its definition in Eq. (20).

4.3.1 Algorithmic momentum conservation

According to [2], it can be verified that the cG(k) method conserves the total linear and angular momenta inherently when using the k-point Gaussian quadrature. As already mentioned above, the key of this conservation is the fulfilled collocation property by the k-point Gaussian quadrature in connection with the chosen trial function in Eq. (51).

4.4 The enhanced Galerkin (eG) time stepping scheme

The equations in this section mainly refer to the works [2] and [1], where the equations are derived for isotropic material elaborately. We therefore only summarize here the main results, which are still valid since structural tensors are time-independent.

In general, the cG time-stepping schemes from the section above does not conserve mechanical energy, but only in the case that the integral in Eq. (57) is calculated exactly. This requirement is called the energy conservation condition for the cG(k) method, from which we can derive a design criterion that leads finally to the enhanced Galerkin (eG) time-stepping scheme.

Further, the so-called *assumed strain approximation* $\mathbf{C}_e$ is used, where the right CAUCHY–GREEN tensor is approximated directly by its nodal values $\mathbf{C}_I^e$ at the time nodes α_I (see also [4]). This approximation is indifferent with respect to rigid body motions (cf. [14]), and given by

$$\mathbf{C}_e = \sum_{l=1}^{k+1} M_I(\alpha) \mathbf{C}_I^e \qquad (59)$$

Furthermore, the design criterion for energy conservation leads to an enhanced gradient of the strain energy density function W_e. Considering the *assumed strain approximation* from Eq. (59), one can find a so-called *enhanced assumed gradient* associated with k-point Gaussian quadrature that reads

$$\underline{\mathbf{D}} W_e = \nabla_{\mathbf{C}_e} W_e[\mathbf{C}_e(\alpha), \mathbf{A}] + \frac{\mathscr{G}_e}{\underline{\mathscr{N}_e}} \frac{\partial \mathbf{C}_e(\alpha)}{\partial \alpha} \qquad (60)$$

with the terms

$$\underline{\mathscr{G}_e} = W_e[\mathbf{C}_e(1), \mathbf{A}] - W_e[\mathbf{C}_e(0), \mathbf{A}]$$

$$- \sum_{l=1}^k \nabla_{\mathbf{C}_e} W_e[\mathbf{C}_e(\xi_l), \mathbf{A}] : \frac{\partial \mathbf{C}_e(\xi_l)}{\partial \alpha} w_l \qquad (61)$$

$$\underline{\mathscr{N}_e} = \sum_{l=1}^k \frac{\partial \mathbf{C}_e(\xi_l)}{\partial \alpha} : \frac{\partial \mathbf{C}_e(\xi_l)}{\partial \alpha} w_l \qquad (62)$$

When inserting the enhanced assumed gradient in the cG(k) method, the eG(k) method is obtained. These higher-order energy and momentum conserving time-stepping schemes read

$$\sum_{J=1}^{k+1} \int_0^1 \tilde{M}_I M_J' \, d\alpha \mathbf{q}_J - h_n \int_0^1 \tilde{M}_I \mathbb{M}^{-1} \mathbf{p} \, d\alpha = \mathbf{0} \tag{63}$$

$$\sum_{J=1}^{k+1} \int_0^1 \tilde{M}_I M_J' \, d\alpha \mathbf{p}_J + h_n \int_0^1 \tilde{M}_I \left(\underline{\mathbb{Q}} \mathbf{q} - \mathbf{f}_{nc} \right) d\alpha = \mathbf{0} \tag{64}$$

with $I = 1, \ldots, k$, where the second integral in Eq. (64) is calculated by

$$\int_0^1 \tilde{M}_I \left(\underline{\mathbb{Q}} \mathbf{q} - \mathbf{f}_{nc} \right) d\alpha$$
$$= \sum_{l=1}^{k} \tilde{M}_I(\xi_l) \left[\underline{\mathbb{Q}}(\xi_l) \mathbf{q}(\xi_l) - \mathbf{f}_{nc}(\xi_l) \right] w_l \tag{65}$$

The time approximation $\underline{\mathbb{Q}}(\alpha)$ of the stiffness matrix is given by the element stiffness matrices $\underline{\mathbb{Q}}_e(\alpha)$ with the entries

$$\underline{\mathbb{Q}}_{ab}^e = \int_{\mathcal{B}_0^e} 2 \underline{\mathbf{D}} W_e(\alpha) : \mathbf{N}_{ab}^e \, dV \tag{66}$$

using the enhanced assumed gradient.

5 Representative numerical examples

In this section, we present representative numerical examples using the eG(k) time stepping schemes as well as the cG(k) schemes for $k = 1, 2, 3$. We consider both a free moving structure and a supported structure with DIRICHLET boundary conditions. The latter is excited by a transient external force (see [17] for static numerical experiments, for instance). Our aim is to verify the conservation properties stated for the eG(k) method, and to present a comparison between the cG(k) and the eG(k) method with respect to conservation of first integrals, accuracy and numerical cost.

5.1 COOK's membrane

As first example, we consider the well-known example for anisotropic stress behaviour of COOK's membrane, here discretized by $n_{el} = 100$ eight-node LAGRANGE elements, and defined by $n_{no} = 242$ spatial element nodes (cf. [24]). The membrane is clamped on its left edge and loaded by the force $\mathbf{F}$ on the right edge, which is uniformly distributed on all nodes and acts in y-direction. The direction of the force is fixed and not influenced by the deformation of the membrane. The initial position is equal to the undeformed reference
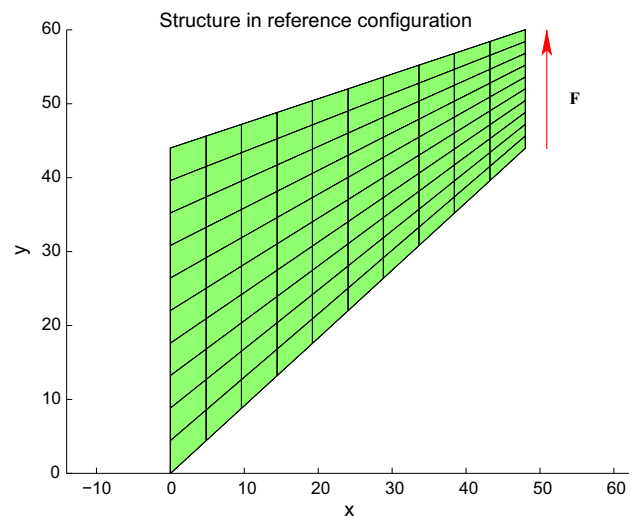
Fig. 1 Initial configuration of the left side clamped COOK's membrane

configuration in Fig. 1. We consider both a simple static load, where the membrane is loaded by a time-independent force, and a transient dynamic load, where we have a hat-shaped excitation combined with a certain initial velocity field. More precisely, in the static load case, the nodal forces $\mathbf{F}^A$, $A \in \{1, \ldots, n_{no}\}$, of the right boundary elements are given by

$$\mathbf{F}^A = \hat{\mathbf{F}} = \text{const.} \tag{67}$$

where $\hat{\mathbf{F}}$ denotes the y-direction vector weighted with an amplitude $\|\hat{\mathbf{F}}\|$, and in the dynamic load case, the force is time-dependent, and described by the hat function

$$f(t) = \begin{cases} t & \text{at } 0 \leq t \leq 1 \\ 2 - t & \text{at } 1 < t \leq 2 \\ 0 & \text{at } t > 2 \end{cases}$$

such that

$$\mathbf{F}^A = \hat{\mathbf{F}} \cdot f(t) \tag{68}$$

Furthermore, we have an initial velocity field with components in the y-direction whose magnitude increases linearly from the left to the right edge, which means the A-th node with its coordinate vector $\mathbf{q}^A = [x^A, y^A, z^A]^T$ has an initial velocity vector

$$\mathbf{v}^A = \left[0, v_{max} \cdot \frac{x^A}{48}, 0 \right]^T \tag{69}$$

where the value of v_{max} is generally set to 1.

The considered mechanical structure consists of transversally isotropic continuous material with a homogeneous mass density $\rho_0 = 1$. Its mechanical behaviour is defined by the strain energy density function
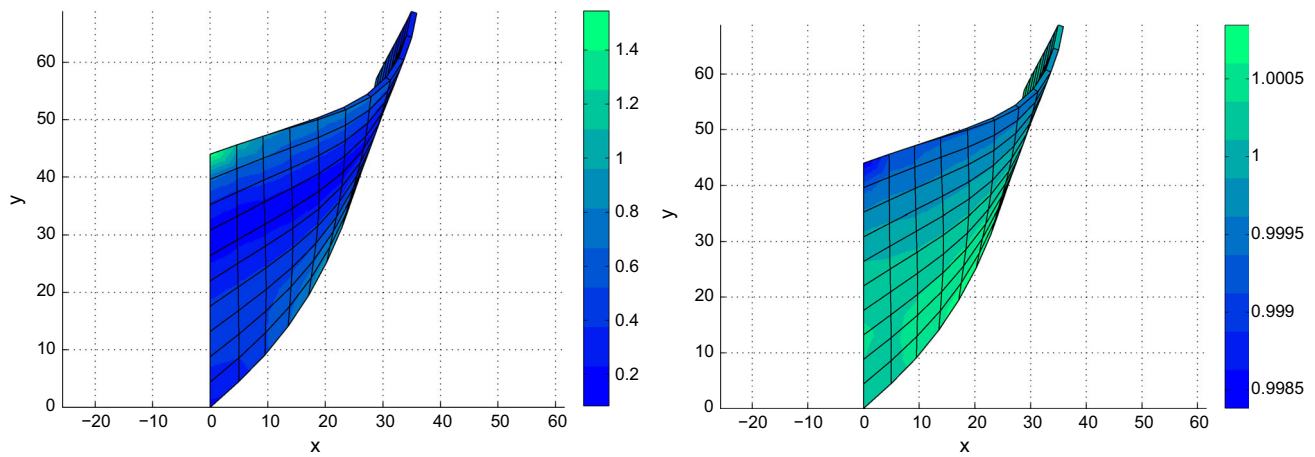
Fig. 2 Static deformation of COOK's membrane due to a static force with absolute value $\|\hat{\mathbf{F}}\| = 400$ using the non-stiff material. The *colours* indicate in the *left plot* the Eucidean norm $\|\tau\|_2$ of the KIRCHHOFF stress tensor and in the *right plot* the third invariant I_3. (Color figure online)

$$W = W^{\text{isotr}} + W^{\text{aniso}} \tag{70}$$

with

$$W^{\text{isotr}} = \frac{c_1}{2}\left(I_3^{-1/3} I_1 - 3\right) + c_2\left(I_3^{-1} I_2^{3/2} - 3\sqrt{3}\right) + c_3 (I_3 - 1)^2 \tag{71}$$

$$W^{\text{aniso}} = \frac{c_4}{2c_5}\exp\left[c_5\left(I_3^{-1/3} I_4 - 1\right)^2 - 1\right] \tag{72}$$

where the parameters c_1, c_2, c_3 and c_4 are stress-like parameters, while the parameter c_5 is dimensionless (see Reference [33] and Reference [34], respectively, and note Remark 2 and Remark 3). We define a parameter set for the non-stiff case with the values

$$c_1 = 300$$
$$c_2 = 100$$
$$c_3 = 100$$
$$c_4 = 240$$
$$c_5 = 80$$
$$\|\hat{\mathbf{F}}\| = 220 \tag{73}$$

and a set for the stiff case, given by

$$c_1 = 3000$$
$$c_2 = 1000$$
$$c_3 = 1000$$
$$c_4 = 2400$$
$$c_5 = 800$$
$$\|\hat{\mathbf{F}}\| = 2200 \tag{74}$$

The direction vector for the reinforced fibres takes the form $\mathbf{a} = [1, 1, 1]^T/\sqrt{3}$.

Remark 2 The isotropic strain energy function in Eq. (71) can be found in Reference [33] with the applicability only for deformations with $\det[\mathbf{F}] \approx 1$ as calculated during the considered deformations in this paper. We refer to this reference for an appropriate modification of Eq. (71) for larger deformations.

Remark 3 The anisotropic strain energy function in Eq. (72) has been taken from Reference [34] due to the guaranteed vanishing second PIOLA–KIRCHHOFF stress tensor $\mathbf{S}$ in the reference configuration $\mathscr{B}_0$, and therefore also in the case of rigid body motions. This is crucial for the applicability of the enhanced assumed gradient $\underline{\mathbf{D}}W_e(\alpha)$ used in this paper, as well as for its scientific basis, the discrete gradient in [14]. But, note that this function is only polyconvex for the range $I_3^{-1/3} I_4 > 1$, in contrast to the strain energy function proposed in [34]. However, as also mentioned in Reference [34], for the proposed strain energy function the vanishing stress has to be enforced in the reference configuration mathematically, and in the present paper also for the superimposed group motions as translations and rotations.

5.1.1 Numerical results

In Fig. 2, the static deformation of the membrane due to the force $\|\hat{\mathbf{F}}\| = 400$ is depicted, which is an examplary representation of the effect of the anisotropic fibre direction (cf. [24]). In the left plot, the colours of the spatial finite elements indicate the distribution of the Euclidean norm of the KIRCHHOFF stress tensor. We observe a higher total stress (fibres and matrix) at the boundaries of the membrane. The right plot demonstrates the distribution of the third invariant I_3 of the membrane material. Here, we show that the material parameter are chosen so that $\det[\mathbf{C}] \approx 1.0$.

Fig. 3 shows a representative configuration of the nonstiff membrane (here at time $t = 2$) during the dynamic simula-
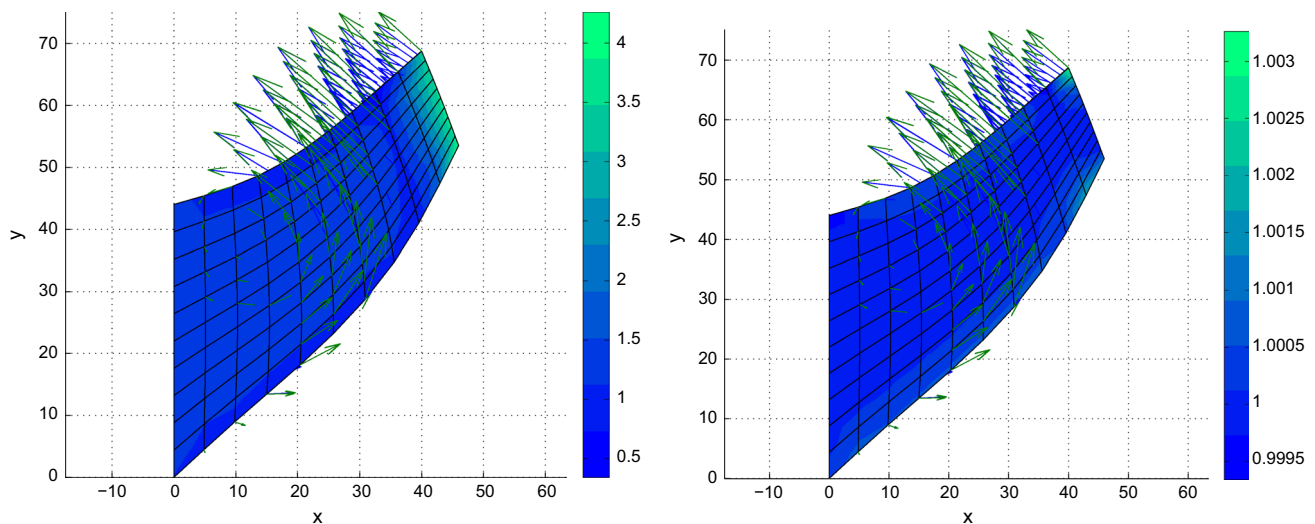
Fig. 3 Dynamic deformation of COOK's membrane at time $t_{20} = 2$ in the dynamic load case using the non-stiff material determined by the cG(1) method with the time step size $h_n = 0.1$. The *colours* indicate

in the *left plot* the Eucidean norm $\|\tau_{20+1/2}\|_2$ of the KIRCHHOFF stress tensor and in the *right plot* the third invariant $I_{3_{20+1/2}}$. (Color figure online)

tion, calculated by the cG(1) method with the time step size $h_n = 0.1$. In the left plot, we show the current distribution of the norm of the KIRCHHOFF stress tensor at the first temporal GAUSS point, that is the midpoint of the time step. We observe a high total stress at the loaded boundary of the membrane. The arrows at the element nodes demonstrate the current LAGRANGIAN velocity field during the oscillation. The right plot depicts the current distribution of the third invariant I_3 of the membrane material. Here, we observe that the material parameter are chosen so that $\det[\mathbf{C}] = 1.0 \pm 0.5\%$.

In the dynamic load case, computed in a transient long term simulation, the total linear and total angular momenta of the membrane cannot be constant. The dynamic reaction forces on the left edge of the membrane have to be considered in the momentum balances, and effect a temporal change of the momenta during the oscillation of the membrane. Due to the oscillation excitation until the time $t = 2$, the total energy increases to a certain value and can be investigated with respect to energy conservation from the time $t \geq 2$ on.

Figures 4, 5 and 6, respectively, depict a comparison of the total energies of the cG(k) and the corresponding eG(k) method of the non-stiff material. We recognize, that after the changes of the time step sizes h_n from 0.1 to 1, the total energies of the cG(k) time-stepping schemes increase up to certain values, and then the simulations are aborted due to blow-up-behaviour of the mechanical structures. We have to change the time step sizes up to the tenfold value to enforce aborts of the cG(k) time-stepping schemes, because during the oscillations of the membranes one has rigid body rotations which are not as large as those of the blade. This observation is also reported in Reference [35] by using the standard trapezoidal rule. Considering the eG(k) time-stepping schemes in the non-stiff case, the total energies again remains exactly
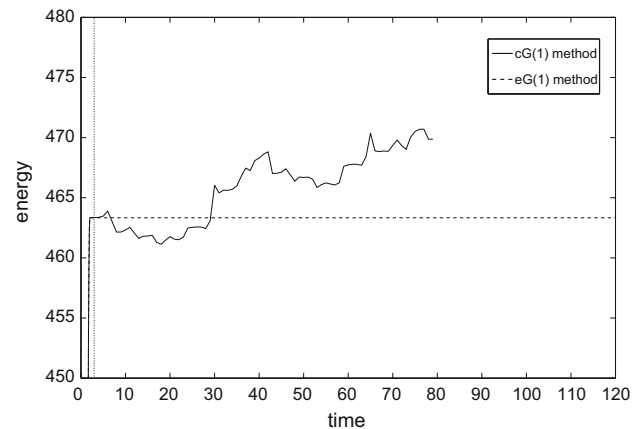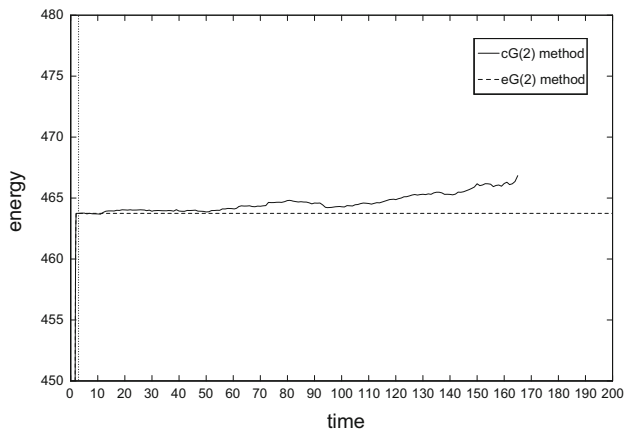

Fig. 4 Comparison of the total energy H using the cG(1)-method and the eG(1)-method in the non-stiff case. The time step size is 0.1 for $t \leq 3$ and 1 for $t > 3$

constant after the excitation, and are indifferent with respect to time step size changes.

We now compare the total energies of the cG(k) and the corresponding eG(k) method when using the stiff material, depicted in Figs. 7, 8 and 9. For the polynomial degrees $k = 1$ and $k = 2$, the time step size h_n was changed from 0.1 to 0.2. For $k = 3$, the time step size was increased from 0.1 up to 1. We recognize again that the eG(k) schemes conserve the total energies exactly after the excitation, while the cG(k) schemes abort at a certain simulation time. Further, the time step changes demonstrate the benefit of higher-order time integrators as the cG(k) and eG(k) method on numerical stability.

Figures 10 and 11 depict the logarithm of the relative global error in the position at time $T = 1$ versus the logarithm of the associated time step size h_n, and the double logarithmic plot of the relative global error

Fig. 5 Comparison of the total energy H using the cG(2)-method and the eG(2)-method in the non-stiff case. The time step size is 0.1 for $t \leq 3$ and 1 for $t > 3$
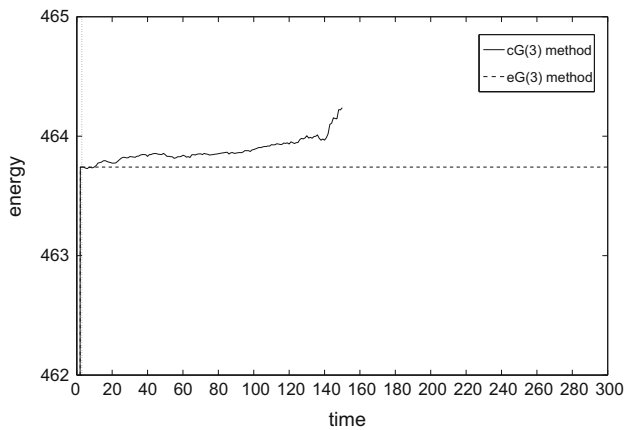

Fig. 6 Comparison of the total energy H using the cG(3)-method and the eG(3)-method in the non-stiff case. The time step size is 0.1 for $t \leq 3$ and 1 for $t > 3$
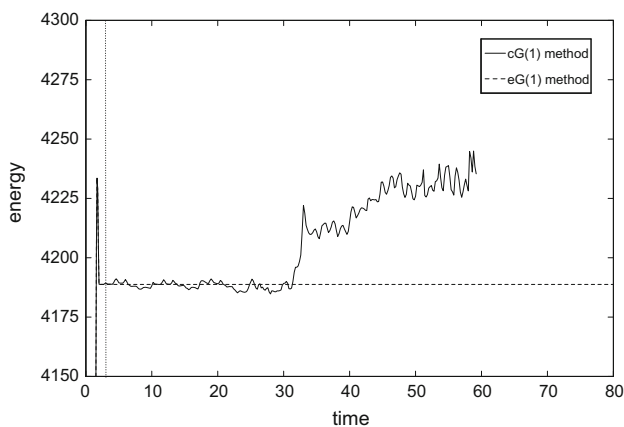

Fig. 7 Comparison of the total energy H using the cG(1)-method and the eG(1)-method in the stiff case. The time step size is 0.1 for $t \leq 3$ and 0.2 for $t > 3$

$$e_{\mathbf{q}} = \frac{\|\mathbf{q}(T) - \mathbf{q}^{\mathrm{ref}}(T)\|}{\|\mathbf{q}^{\mathrm{ref}}(T)\|} \tag{75}$$
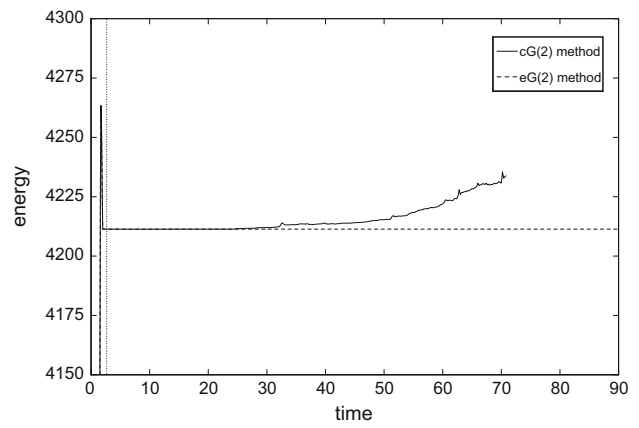
Fig. 8 Comparison of the total energy H using the cG(2)-method and the eG(2)-method in the stiff case. The time step size is 0.1 for $t \leq 3$ and 0.2 for $t > 3$
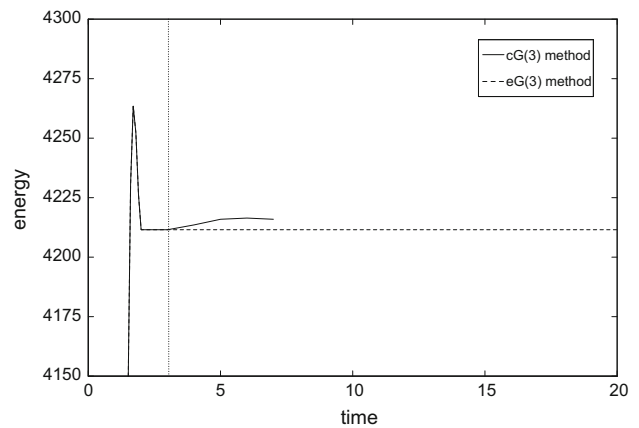
Fig. 9 Comparison of the total energy H using the cG(3)-method and the eG(3)-method in the stiff case. The time step size is 0.1 for $t \leq 3$ and 1 for $t > 3$

versus the corresponding CPU time, respectively. The reference solution $\mathbf{q}^{\mathrm{ref}}$ is again computed using the eG(4) method with a time step size of $h_n = 0.001$. Both diagrams show relations with respect to the convergence and the numerical costs that are similar to those of the simulation of the blade's free flight in the next section.

5.2 Free flight of a fibre-reinforced blade

As second example, we consider a fibre-reinforced blade discretized by $n_{\mathrm{el}} = 100$ eight-node LAGRANGE elements in space, which are defined by $n_{\mathrm{no}} = 238$ element nodes (cf. [2]). The centre of the blade's hub is positioned in the origin of the respective Euclidean space. The initial position is equal to the undeformed reference configuration. The structure consists of transversally isotropic continuous material with a homogeneous unit mass density $\rho_0 = 1$. Its mechanical behaviour is defined by the following strain energy density function
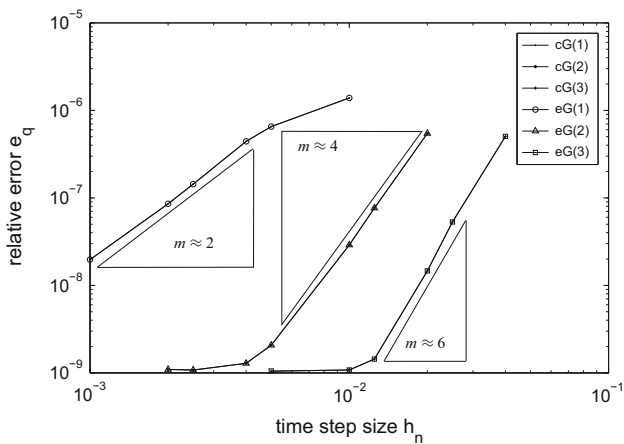
Fig. 10 Relative global error in the position $e_{\mathbf{q}}$ versus time step size h_n in the non-stiff case ($T = 1$)
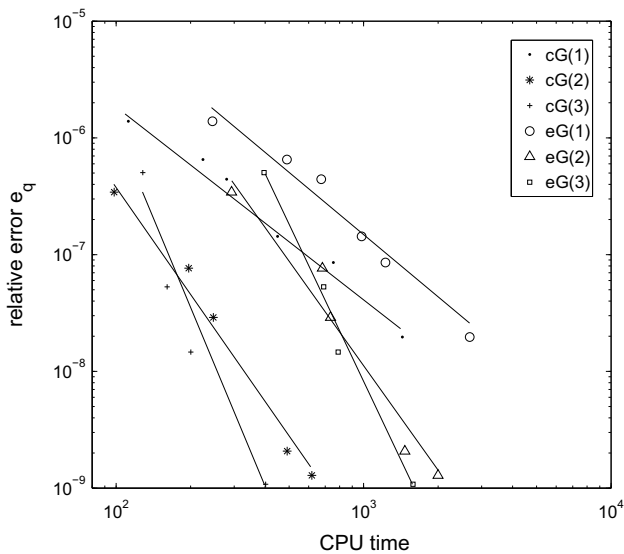
Fig. 11 Relative global error in the position $e_{\mathbf{q}}$ versus CPU time in the non-stiff case ($T = 1$)
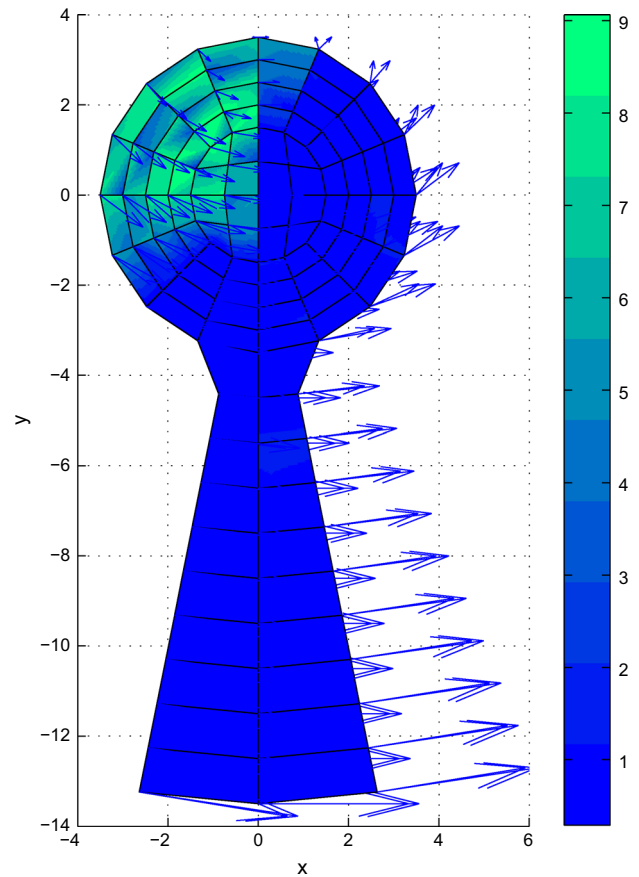
$$W = W^{\text{isotr}} + W^{\text{aniso}} \tag{76}$$

with

$$W^{\text{isotr}} = \frac{c_1}{2}(I_3^{-\frac{1}{3}} I_1 - 3) + c_2(I_3 - 1)^2 \tag{77}$$

$$W^{\text{aniso}} = \frac{c_3}{2c_4} \exp\left[c_4 \left(I_3^{-1/3} I_4 - 1 \right)^2 - 1 \right] \tag{78}$$

where the parameters c_1, c_2 and c_3 are stress-like parameters, while the parameter c_4 is dimensionless. We define a parameter set for the non-stiff case with the values

$$c_1 = 300$$
$$c_2 = 100$$
$$c_3 = 240$$
$$c_4 = 80 \tag{79}$$

Fig. 12 Initital configuration $\mathscr{B}_0$ of the fibre-reinforced blade in the non-stiff case. The *colour* indicates the Euclidean norm $\|\tau_{0+1/2}\|_2$ of the KIRCHHOFF stress tensor determined by the cG(1) method. (Color figure online)

and one for the stiff case with

$$c_1 = 3000$$
$$c_2 = 1000$$
$$c_3 = 2400$$
$$c_4 = 800 \tag{80}$$

The used exemplary unit direction vector of the fibres in the polymer matrix reads $\mathbf{a} = [1, 1, 1]^T/\sqrt{3}$.

The fibre-reinforced blade performs a free flight due to its initial translational velocity described by the vector $\mathbf{v}_T = [2, 0, -0.1] \in \mathbb{R}^3$ and its initial angular velocity vector $\omega_0 = [0, 0.7, 0.7] \in \mathbb{R}^3$ such that the initial velocity vector of the node A is determined by means of the EULER theorem as

$$\mathbf{v}_0^A = \mathbf{v}_T + \omega_0 \times \mathbf{q}_0^A \tag{81}$$

The initial configuration $\mathscr{B}_0$ with the initial Lagrangian velocity field $\mathbf{v}_0$ is depicted in Fig. 12. This chosen velocity field causes a total (fibers and matrix) KIRCHHOFF stress $\|\tau_{0+1/2}\|_2$ at the midpoint of the first time step, indicated by the depicted colours in Fig. 12.
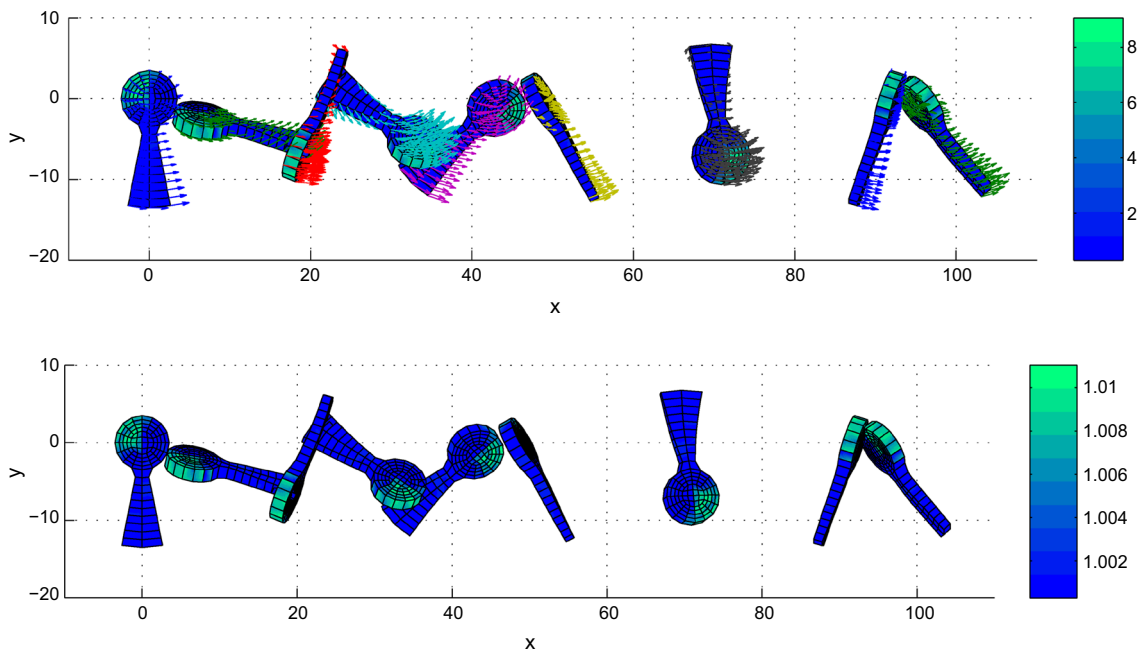
Fig. 13 Current configurations $\mathcal{B}_{t_n}$ of the fibre-reinforced blade in the non-stiff case, starting at $t_0 = 0$ on the left and finishing at $t_N = 19.6$ on the right, determined by the cG(1) method. The *colour* indicates in the *top plot* the Eucidean norm $\|\tau_{n+1/2}\|_2$ of the KIRCHHOFF stress tensor and in the *bottom plot* the third invariant $I_{3_{n+1/2}}$. The *arrows* in the *top plot* denotes the current Lagrangian velocity field. (Color figure online)
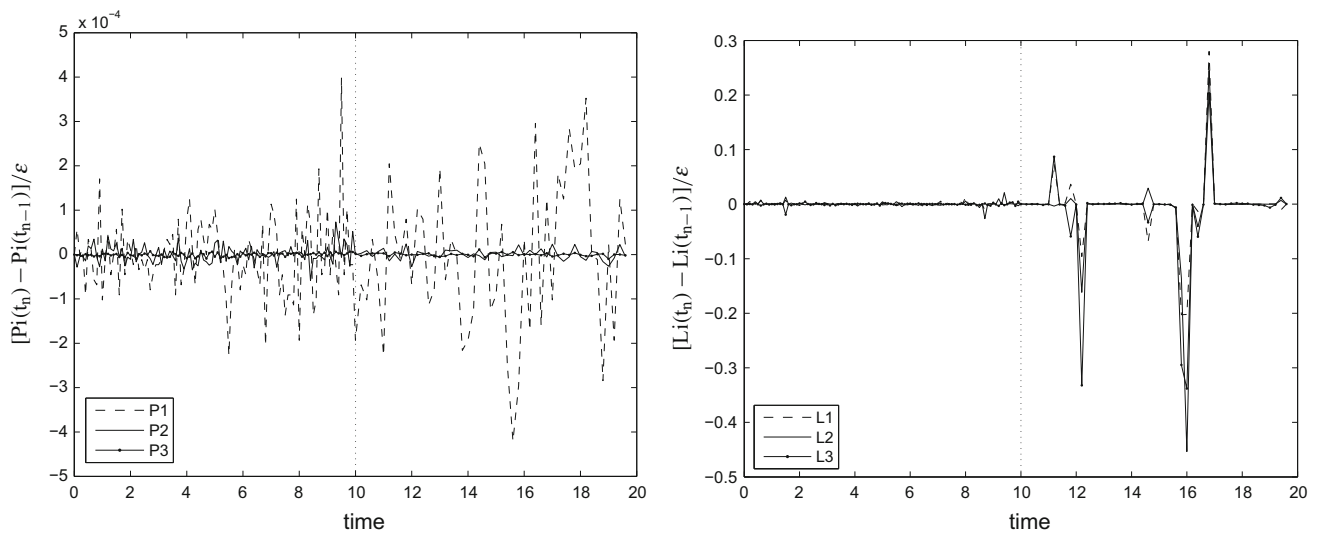
Fig. 14 Time step differences of the total linear and angular momenta relative to the tolerance $\epsilon = 10^{-8}$ of the NEWTON–RAPHSON pertaining to the fibre-reinforced blade computed with the cG(1)-method in the non-stiff case. The time step size h_n is 0.1 for $t \leq 10$ and 0.2 for $t > 10$

5.2.1 Numerical results

An examplary motion of the fibre-reinforced blade using the non-stiff material determined by the cG(1) method is depicted in Fig. 13. In the top plot, we show the time evolution of the norm of the KIRCHHOFF stress tensor at the first temporal GAUSS point of the cG(1) method, i.e. the midpoint of the time step, as colours of the spatial elements. We observe a high total stress in a quarter of the blade's hub, caused by

the given initial velocity field in connection with the inertia of the blade. The arrows at the element nodes indicates the current Lagrangian velocity field of the blade. The bottom plot demonstrates the time evolution of the third invariant I_3 of the blade material. Here, we show that the material parameter are chosen so that $\max(\det[\mathbf{C}]) = 1.0 + 1\%$.

In Fig. 14, we show the time step differences of the total linear and the total angular momenta of the cG(1) method in the non-stiff case relative to the NEWTON–RAPHSON toler-
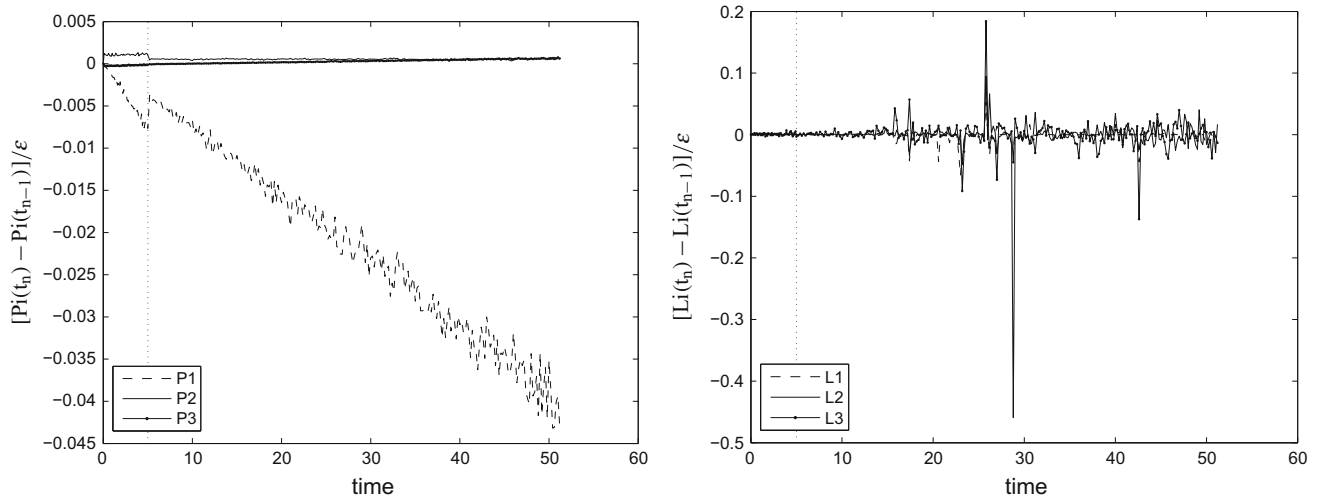
Fig. 15 Time step differences of the total linear and angular momenta relative to the tolerance $\epsilon = 10^{-8}$ of the NEWTON–RAPHSON pertaining to the fibre-reinforced blade computed with the cG(2)-method in the non-stiff case. The time step size h_n is 0.1 for $t \leq 5$ and 0.2 for $t > 5$
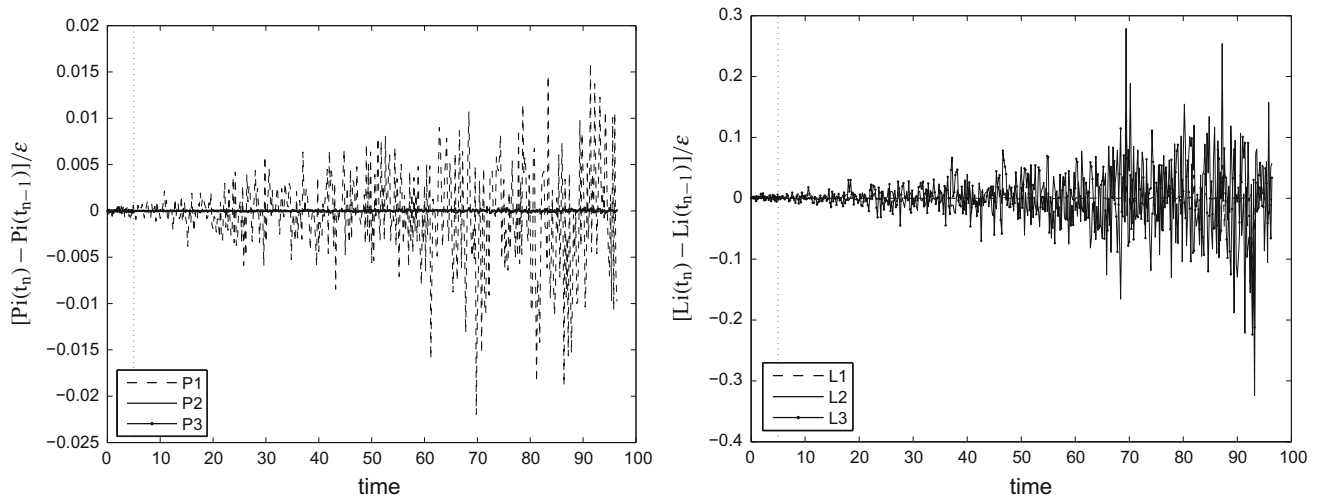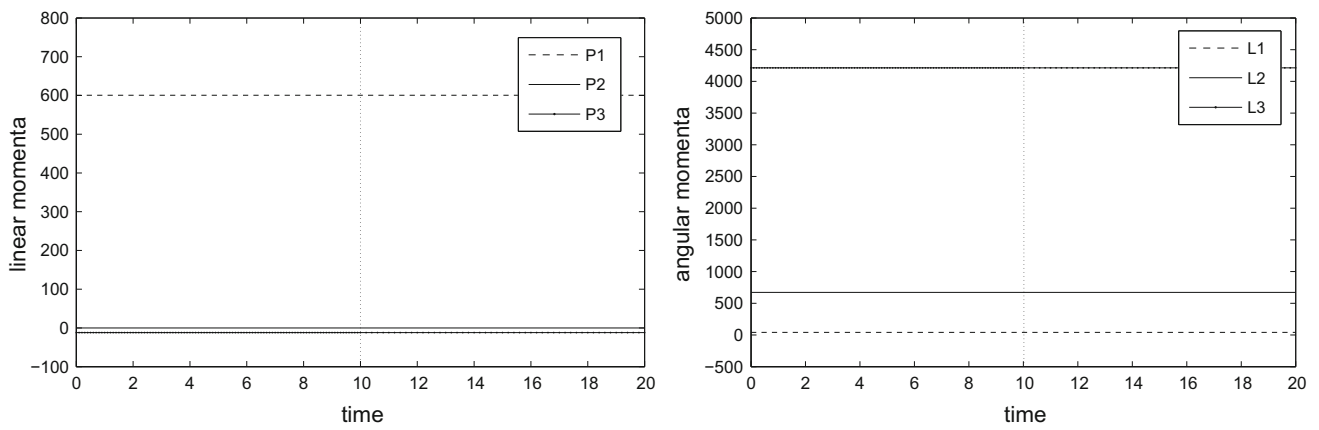

Fig. 16 Time step differences of the total linear and angular momenta relative to the tolerance $\epsilon = 10^{-8}$ of the NEWTON–RAPHSON pertaining to the fibre-reinforced blade computed with the cG(3)-method in the non-stiff case. The time step size h_n is 0.1 for $t \leq 5$ and 0.2 for $t > 5$

ance $\epsilon = 10^{-8}$. Algorithmic momentum conservation now means that this time evolutions stay below a corresponding absolute value of one. Since the cG(1) method shows an absolute value below $5 \cdot 10^{-4}$ for the total linear momenta and 0.3 for the total angular momenta, the algorithmic momentum conservation of the cG(1) method is obvious. But the comparison with the higher-order cG-methods furnishes an

Table 1 Comparison of the time step differences of the total linear and the total angular momenta of the cG method relative to the NEWTON–RAPHSON tolerance $\epsilon = 10^{-8}$

|	$\frac{[Pi(t_n) - Pi(t_{n-1})]}{\epsilon}$	$\frac{[Li(t_n) - Li(t_{n-1})]}{\epsilon}$
cG(1)	$\mathcal{O}(10^{-4})$	$\mathcal{O}(10^{-1})$
cG(2)	$\mathcal{O}(10^{-3})$	$\mathcal{O}(10^{-1})$
cG(3)	$\mathcal{O}(10^{-2})$	$\mathcal{O}(10^{-1})$

interesting result. The algorithmic conservation for quadratic (see Fig. 15) and cubic (see Fig. 16) time finite elements still apply, but the range of the absolute value for the total linear momentum difference on the time step increases, in contrast to the range of the total angular momentum difference (see Table 1). This behaviour of the total linear momentum is attributed to the standard update formula of the nodal momenta $\mathbf{x}_p$ in Eq. (102), which is naturally based on the position vector $\mathbf{x}_q$ of the NEWTON–RAPHSON method (see Appendix 3). An improvement can be reached by an update formula for the momentum vector $\mathbf{x}_p$ directly based on the residual vector $\mathbf{R}(\mathbf{x}_q)$ (more precisely, the vector $\mathbf{F}_{\text{dyn}}$ in Reference [35]). However, this behaviour of the total linear momentum difference can be avoided by solving for the vector $\mathbf{x}_z^T = [\mathbf{x}_q^T, \mathbf{x}_p^T]$ in the NEWTON–RAPHSON scheme. Fore more details, we may refer to the follow up paper.

Fig. 17 Total linear and angular momenta of the fibre-reinforced blade computed with the eG(1)-method in the stiff case. The time step size h_n is 0.1 for $t \leq 10$ and 0.2 for $t > 10$
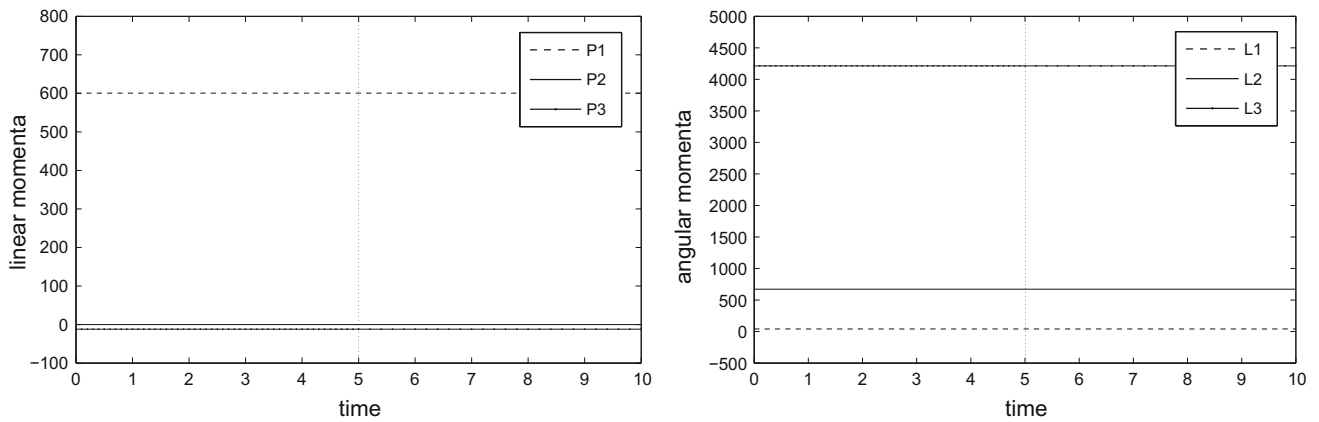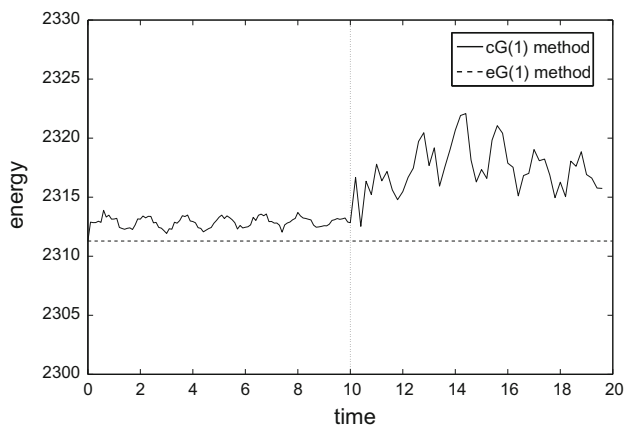

Fig. 18 Total linear and angular momenta of the fibre-reinforced blade computed with the eG(2)-method in the stiff case. The time step size h_n is 0.1 for $t \leq 5$ and 0.2 for $t > 5$
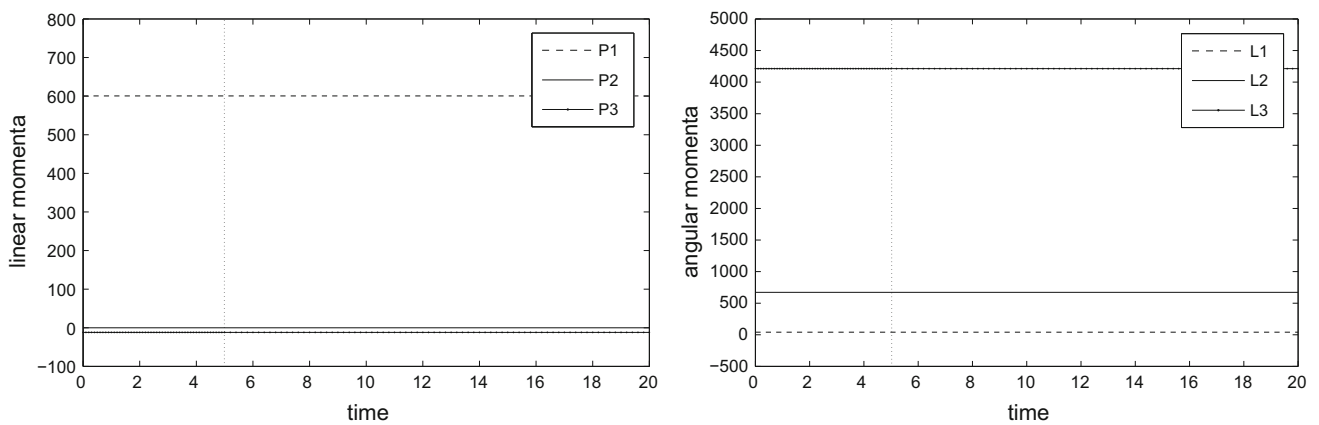

Fig. 19 Total linear and angular momenta of the fibre-reinforced blade computed with the eG(3)-method in the stiff case. The time step size h_n is 0.1 for $t \leq 5$ and 0.2 for $t > 5$
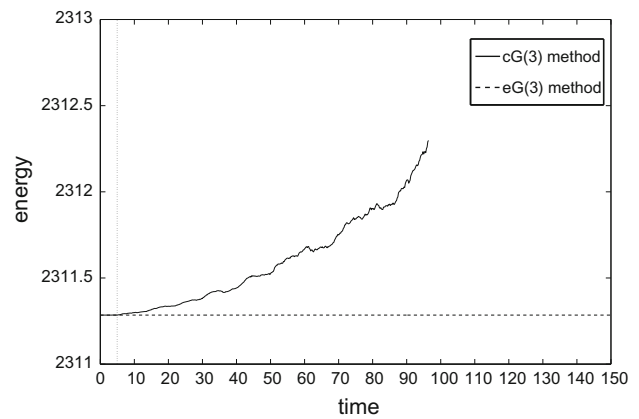
Fig. 20 Comparison of the total energy H using the cG(1)-method and the eG(1)-method in the non-stiff case. The time step size is 0.1 for $t \leq 10$ and 0.2 for $t > 10$

Fig. 22 Comparison of the total energy H using the cG(3)-method and the eG(3)-method in the non-stiff case. The time step size is 0.1 for $t \leq 5$ and 0.2 for $t > 5$
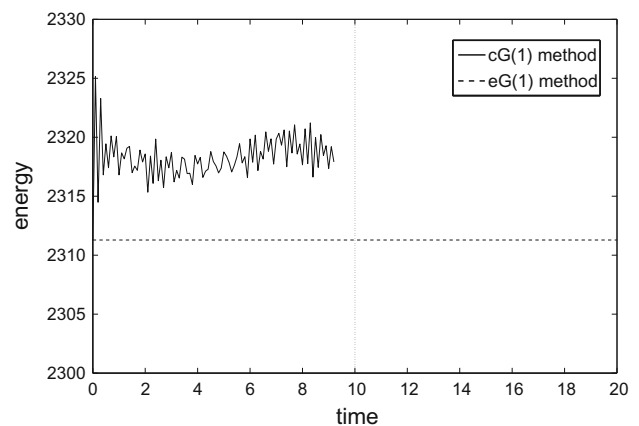

Fig. 21 Comparison of the total energy H using the cG(2)-method and the eG(2)-method in the non-stiff case. The time step size is 0.1 for $t \leq 5$ and 0.2 for $t > 5$
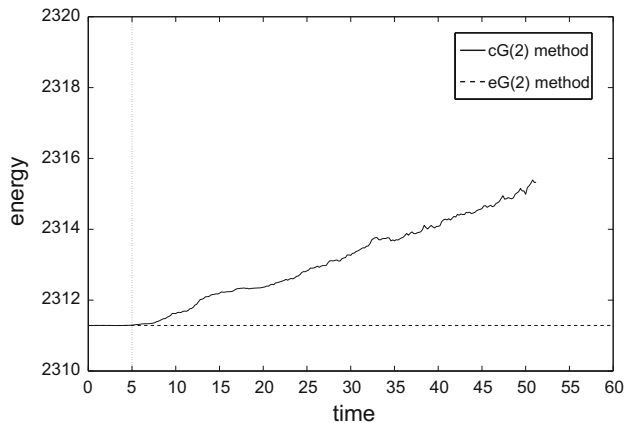
Fig. 23 Comparison of the total energy H using the cG(1)-method and the eG(1)-method in the stiff case. The time step size is 0.1 for $t \leq 10$ and 0.2 for $t > 10$

Considering the algorithmic conservation laws of the simulation using the eG(k)-method in the Figs. 17, 18 and 19, we notice that the enhanced time stepping schemes also conserve both the total linear and the total angular momenta. In general, the fulfillment of the algorithmic conservation laws for total momenta does not depend on the time step size or its change during the simulation. Furthermore, it is not influenced by the transversally isotropic material behaviour.

Regarding the total energies H of the non-stiff material computed by the cG(k) and the eG(k)-method shown in the Figs. 20, 21 and 22, we recognize that after the changes of the time step sizes h_n from 0.1 to 0.2, the total energies of the cG(k) time-stepping scheme increase up to a certain value, and then the simulations are aborted, because the convergence criteria of the applied NEWTON–RAPHSON methods cannot be reached. Here, we detect the so-called blow-up-behaviour of the mechanical structure. With respect to the degree k, it can be seen that the abort of the simulations appear as later as higher k is. This is natural, because

higher-order polynoms in time are able to approximate the overlaid translational and rotational motion of the blade, especially the rigid body rotations, more precisely. On the other hand, considering the eG(k) time-stepping schemes, the total energies remain exactly constant during the complete simulations, and are indifferent with respect to time step size changes.

We now compare the total energies of the cG(k) and the corresponding eG(k) method when using the stiff material, depicted in Figs. 23, 24 and 25. Especially considering the cG(1) method in Fig. 23, one can see that the conventional time-stepping schemes abort after some seconds even with a time step size of 0.1 in the presence of stiffness. Higher-order cG(k) methods abort shortly after the change of the time step size, while the eG(k) schemes again conserve the total energy of the mechanical structure all over the time interval. To give a conclusion about the quality of the reached convergence behaviour of the NEWTON–RAPHSON method, we show an investigation of the relative global error
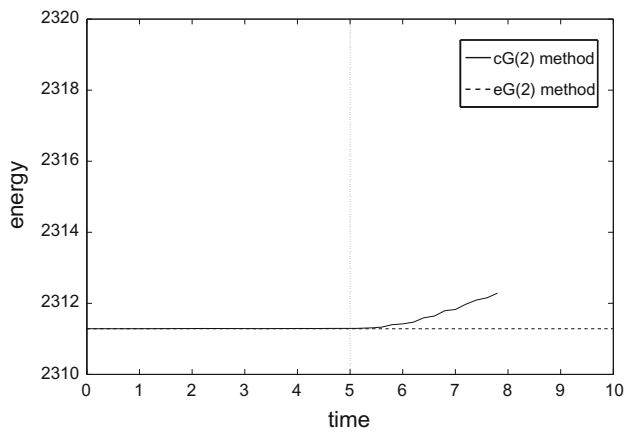
Fig. 24 Comparison of the total energy H using the cG(2)-method and the eG(2)-method in the stiff case. The time step size is 0.1 for $t \leq 5$ and 0.2 for $t > 5$

Fig. 25 Comparison of the total energy H using the cG(3)-method and the eG(3)-method in the stiff case. The time step size is 0.1 for $t \leq 5$ and 0.2 for $t > 5$
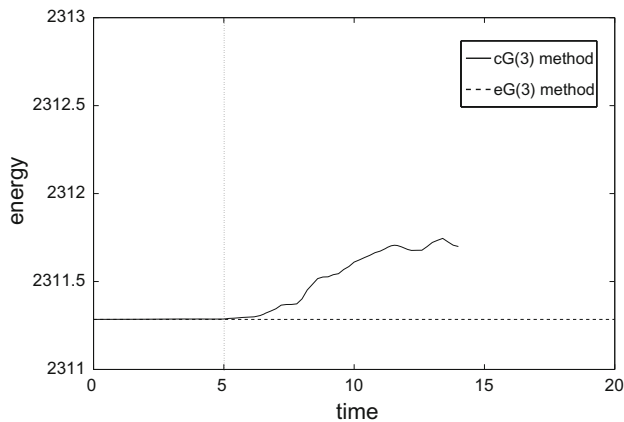
$$e_{\mathbf{q}} = \frac{\|\mathbf{q}(T) - \mathbf{q}^{\mathrm{ref}}(T)\|}{\|\mathbf{q}^{\mathrm{ref}}(T)\|} \tag{82}$$

in the position vector at a certain time T. Here, $\mathbf{q}^{\mathrm{ref}}$ denotes the reference solution of the position vector computed by using the eG(4) method with a time step size of $h_n = 0.001$. Fig. 26 depicts the logarithm of the relative global error in the position at time $T = 1$ versus the logarithm of the associated time step size h_n for the cG(k) and eG(k) method for $k = 1, 2, 3$. We recognize, that the rates of convergence, specified by the slopes of the graphs, have values of about $2k$ for both the cG and the eG method, as aspected. Finally, Fig. 27 shows a double logarithmic plot of the relative global error versus the corresponding CPU time. In general, we see a greater CPU time for the eG(k) method compared to the corresponding cG(k) method due to the higher costs for computing the stiffness and the tangent matrices. However, we identify intersections in graphs of the higher-order methods
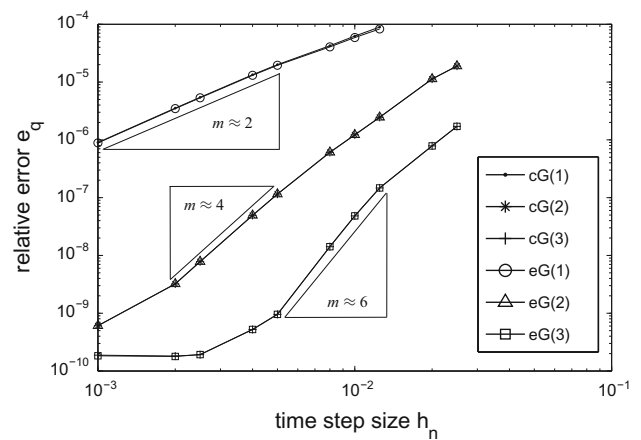
Fig. 26 Relative global error in the position $e_{\mathbf{q}}$ versus time step size h_n in the non-stiff case ($T = 1$)
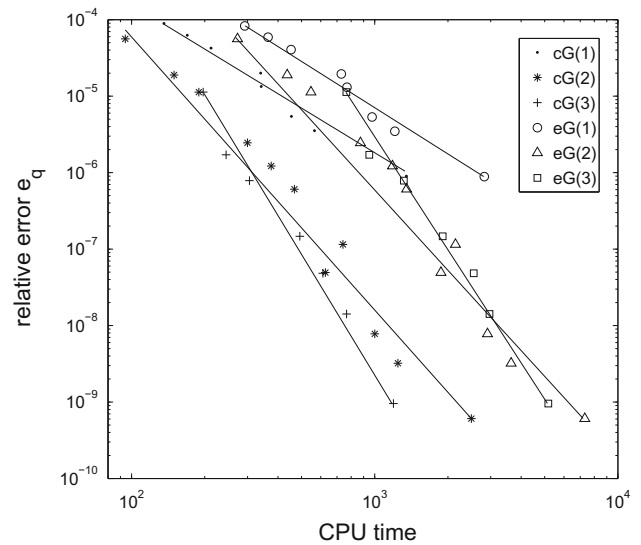
Fig. 27 Relative global error in the position $e_{\mathbf{q}}$ versus CPU time in the non-stiff case (T=1)

($k = 2, 3$), because these methods need less iterations. Thus, higher costs for the computation and assembly of the larger system matrices could be compensated by lower costs in the NEWTON–RAPHSON methods (cf. [35]).

6 Summary and outlook

The relevance of fibre-reinforced polymers (FRP) is steadily increasing in engineering fields due to the possibility of light-weight construction, for example in the aircraft industry [36]. Due to the high strength in fibre direction, but possible large deformations in other directions, these composites replace more and more traditional strong but heavy materials as metals. Fibre-reinforced polymers are often subjected to small strains, but a geometrically nonlinear formulation is neces-

sary due to large deformations of the reinforced structural elements at least in one direction, as for helicopter rotor blades. Here, the fibres have the function to stabilize the structure in one direction in order to counteract large centrifugal forces. A stress analyses of rotor blades in long-run simulations demands numerically stable time integrators for anisotropic materials. This paper presents numerically stable and also higher-order accurate time stepping schemes for nonlinear elastic fibre-reinforced continua with anisotropic stress behaviour. These time-stepping schemes are based on a time discretization of ordinary differential equations of first order. Therefore, a state space representation of the considered continuum dynamics is necessary. In this paper, the Hamiltonian formulation of dynamics is preferred, because two of the first integrals of the motion are at most quadratic approximated in time, i.e. the total momenta, which allows an exact algorithmic total momentum conservation. These algorithmic conservation properties allow for more numerical stability in the presence of large rotations. Since fibre-reinforced polymers are composite materials made of a polymer matrix reinforced with fibres of a different material, these polymers are here modelled for finite strains by an isotropic material law for the matrix, and structural tensors for the fibres (cf. [29,30]). To build such an anisotropic material law, we first define a scalar-valued free energy density function [31], which is a sum of free energy density functions that depend on the scalar-valued invariants of the right CAUCHY–GREEN tensor and the structural tensors, and then derive from that the second PIOLA–KIRCHHOFF stress tensor in the equations of motion. The space-time discretisation of the considered anisotropic continuum is performed by a trilinear BUBNOV–GALERKIN approximation in space, and a higher-order accurate PETROV–GALERKIN approximation in time. In order to preserve the mathematical structure of the equations of motion leading to asymptotically stable discrete nonlinear equations of motion, algorithmic conservation laws of total linear and total angular momentum as well as total energy are preserved by Gaussian quadrature and a special time approximation of the stress tensor. The resulting energy-momentum conserving eG(k) time-stepping schemes are applied to two mechanical structures: a three-dimensional blade-model and the well-known COOK's membrane. Both continuum bodies are reinforced by uni-directional fibres, and are simulated in the presence of large deformations and superimposed rigid body motions. The presented eG(k) time-stepping schemes of higher-order prove to be numerically stable in comparison with the standard cG(k) time-stepping schemes of the same order. Further, the advantage of increasing the polynomial order in dynamical simulations is also shown. In fact, higher-order schemes reduce numerical time integration costs if accuracy is of interest for the simulation, and are more stable in the presence of material stiffness. Accordingly, these schemes can be recommended for sim-

ulating fibre-reinforced continua under dynamic loads as helicopter rotor blades.

In the future, we investigate a new modification of the enhanced assumed gradient $\underline{\mathbf{D}}W_e$, which take the fibre direction $\mathbf{a}$ in the structural tensors not only in its numerator $\mathscr{G}_e$ into account. From this new adjustment to anisotropic material, the authors suspect an important improvement especially for two and more families of fibres. Further, we aim at the incorporation of the mixed spatial finite element discretization in [15], internal damping behaviour of the matrix and the fibres, the thermal conductivity of both, especially of conductive fibres, in nonlinear mechanical structures [37].

Appendix

In the following, the implementation of the presented time-stepping schemes are sketched, including the residuals and the corresponding tangent matrices in the NEWTON–RAPHSON method neccessary for solving these nonlinear algebraic equation systems. In general, the implementation is close to the one in [2].

Appendix 1: The stress tensor

As already derived extensively in [24,38] and [18], the second PIOLA–KIRCHHOFF stress tensor corresponding to the above free energy density function is given by

$$
\begin{aligned}
\mathbf{S}(\mathbf{C}, \mathbf{A}) &= 2\nabla_{\mathbf{C}}W = 2\sum_{i=1}^{5}\frac{\partial W}{\partial I_i}\frac{\partial I_i}{\partial \mathbf{C}}\\
&= 2\left\{ \left(\frac{\partial W}{\partial I_1}+\frac{\partial W}{\partial I_2}I_1\right)\mathbf{I} - \frac{\partial W}{\partial I_2}\mathbf{C} + \frac{\partial W}{\partial I_3}I_3\mathbf{C}^{-1}\right.\\
&\quad \left. + \frac{\partial W}{\partial I_4}\mathbf{A} + \frac{\partial W}{\partial I_5}(\mathbf{A}\cdot\mathbf{C}+\mathbf{C}\cdot\mathbf{A})\right\}
\end{aligned}
\tag{83}
$$

depending on the right CAUCHY–GREEN tensor and the structural tensor. Here, the free energy function is assumed to depend on the invariants $I_1, \ldots, I_5$. If the free energy function depends on the modified invariants $\tilde{I}_1, \ldots, \tilde{I}_5$, we have to take the chain rule of differentiation into account for calculating the partial derivatives in Eq. (83), which leads to

$$
\frac{\partial W}{\partial I_1} = \frac{\partial W}{\partial \tilde{I}_1}\frac{\partial \tilde{I}_1}{\partial I_1} = \frac{\partial W}{\partial \tilde{I}_1}I_3^{-\frac{1}{3}}
\tag{84}
$$

$$\frac{\partial W}{\partial I_2} = \frac{\partial W}{\partial \tilde{I}_2} \frac{\partial \tilde{I}_2}{\partial I_2} = \frac{\partial W}{\partial \tilde{I}_2} I_3^{-\frac{2}{3}} \qquad (85)$$

$$\frac{\partial W}{\partial I_3} = \sum_{\substack{i=1 \\ i \neq 3}}^{5} \frac{\partial W}{\partial \tilde{I}_i} \frac{\partial \tilde{I}_i}{\partial I_3} \qquad (86)$$

$$\frac{\partial W}{\partial I_4} = \frac{\partial W}{\partial \tilde{I}_4} \frac{\partial \tilde{I}_4}{\partial I_4} = \frac{\partial W}{\partial \tilde{I}_4} I_3^{-\frac{1}{3}} \qquad (87)$$

$$\frac{\partial W}{\partial I_5} = \frac{\partial W}{\partial \tilde{I}_5} \frac{\partial \tilde{I}_5}{\partial I_5} = \frac{\partial W}{\partial \tilde{I}_5} I_3^{-\frac{2}{3}} \qquad (88)$$

where we have to bear in mind in the summation convention that there exist no invariant $\tilde{I}_3$.

Appendix 2: The residuum

Here, the implementation of the residuum for both the cG(k) and the eG(k) method is described. The time-stepping schemes take the form of Eqs. (55) and (56) for the cG(k) method, and of Eqs. (63) and (64) for the eG(k) method, where the stiffness matrix $\mathbb{Q}$ is used for the cG(k) method and stiffness matrix $\underline{\mathbb{Q}}$ for the eG(k) method ,respectively. Collecting the unknown coordinates and momenta in the vectors $\mathbf{x}_q = (\mathbf{q}_2, \dots, \mathbf{q}_{k+1})$ and $\mathbf{x}_p = (\mathbf{p}_2, \dots, \mathbf{p}_{k+1})$, the cG($k$) method read in matrix notation

$$\mathbf{b}'' \otimes \mathbf{q}_1 + [\mathbf{A}'' \otimes \mathbf{I}_{n_{\text{dof}}}]\mathbf{x}_q - h_n\{\mathbf{b}' \otimes [\mathbb{M}^{-1}\mathbf{p}_1]$$
$$+ [\mathbf{A}' \otimes \mathbb{M}^{-1}]\mathbf{x}_p\} = \mathbf{0}$$
$$\mathbf{b}'' \otimes \mathbf{p}_1 + [\mathbf{A}'' \otimes \mathbf{I}_{n_{\text{dof}}}]\mathbf{x}_p$$
$$+ h_n[\tilde{\mathbf{W}}(\xi_1, \dots, \xi_k) \otimes \mathbf{I}_{n_{\text{dof}}}]\mathbf{f}(\mathbf{x}_q) = \mathbf{0} \qquad (89)$$

with

$$\tilde{\mathbf{W}} = \begin{bmatrix} \tilde{M}_1(\xi_1) & \dots & \tilde{M}_1(\xi_1) \\ \vdots & & \vdots \\ \tilde{M}_k(\xi_1) & \dots & \tilde{M}_k(\xi_1) \end{bmatrix} \qquad (90)$$

where we defined the following shorthand notations for a compact representation:

$$\mathbf{A}' = \begin{bmatrix} A'_{11} & \dots & A'_{1k} \\ \vdots & & \vdots \\ A'_{k1} & \dots & A'_{kk} \end{bmatrix} \quad \mathbf{A}'' = \begin{bmatrix} A''_{11} & \dots & A''_{1k} \\ \vdots & & \vdots \\ A''_{k1} & \dots & A''_{kk} \end{bmatrix}$$

$$\mathbf{b}' = \begin{bmatrix} b'_1 \\ \vdots \\ b'_k \end{bmatrix} \quad \mathbf{b}'' = \begin{bmatrix} b''_1 \\ \vdots \\ b''_k \end{bmatrix} \qquad (91)$$

with

$$A'_{IJ} = \int_0^1 \tilde{M}_I M_{J+1} \mathrm{d}\alpha \qquad A''_{IJ} = \int_0^1 \tilde{M}_I M'_{J+1} \mathrm{d}\alpha \quad (92)$$

$$b'_I = \int_0^1 \tilde{M}_I M_1 \mathrm{d}\alpha \qquad b''_I = \int_0^1 \tilde{M}_I M'_1 \mathrm{d}\alpha \qquad (93)$$

The force vector $\mathbf{f}(\mathbf{x}_q)$ is given by

$$\mathbf{f}(\mathbf{x}_q) = \begin{bmatrix} [\mathbb{Q}(\mathbf{q}(\xi_1))\mathbf{q}(\xi_1) - \mathbf{f}_{\text{nc}}(\xi_1)]w_1 \\ \vdots \\ [\mathbb{Q}(\mathbf{q}(\xi_k))\mathbf{q}(\xi_k) - \mathbf{f}_{\text{nc}}(\xi_k)]w_k \end{bmatrix} \qquad (94)$$

Note that the non-conservative force vector $\mathbf{f}_{\text{nc}}$ depends explicitly on time t. Its dependence on the normed time α can be obtained by using the inverse function of Eq. (48) and inserting $t(\alpha)$.

Since the unknown momenta are linear combinations of the unknown coordinates, one can eliminate the vector $\mathbf{x}_p$ such that we obtain the residuum

$$\mathbf{R}(\mathbf{x}_q) = \frac{1}{h_n}[\mathbf{A}_m^R \otimes \mathbb{M}]\mathbf{x}_q + \frac{1}{h_n}\mathbf{A}_q^R \otimes [\mathbb{M}\mathbf{q}_1] + \mathbf{A}_p^R \otimes \mathbf{p}_1$$
$$+ h_n[\tilde{\mathbf{W}}(\xi_1, \dots, \xi_k) \otimes \mathbf{I}_{n_{\text{dof}}}]\mathbf{f}(\mathbf{x}_q) = \mathbf{0} \qquad (95)$$

with

$$\mathbf{A}_m^R = \mathbf{A}''[\mathbf{A}']^{-1}\mathbf{A}'' \quad \mathbf{A}_q^R = \mathbf{A}''[\mathbf{A}']^{-1}\mathbf{b}'' \quad \mathbf{A}_p^R = \mathbf{b}'' - \mathbf{A}''[\mathbf{A}']^{-1}\mathbf{b}' \qquad (96)$$

In order to obtain the matrix representation of the eG(k) method, we only have to substitute the stiffness matrix $\underline{\mathbb{Q}}$ for the matrix $\mathbb{Q}$.

Appendix 3: The Newton–Raphson method

The residuum of the cG(k) method respresents a system of nonlinear equations, which has to be solved numerically for determining the unknown coordinates $\mathbf{q}_A$, $A = 2, \dots, k+1$. Therefore, we apply the NEWTON–RAPHSON method, in which we perform a linearization of the nonlinear equation system and solve these equations iteratively with the following iteration formulas, denoting the iteration index by $i = 0, 1, \dots, i_{\max}$:

$$\mathbf{x}_q^{(i+1)} = \mathbf{x}_q^{(i)} - \mathbf{K}_T^{-1}(\mathbf{x}_q^{(i)})\mathbf{R}(\mathbf{x}_q^{(i)}) \qquad (97)$$

where $\mathbf{K}_T(\mathbf{x}_q) = \nabla_{\mathbf{x}_q}\mathbf{R}(\mathbf{x}_q)$ indicates the tangent operator corresponding to the residuum in Eqs. (89), and is given by

$$\mathbf{K}_T(\mathbf{x}_q) = \frac{1}{h_n}[\mathbf{A}_m^R \otimes \mathbb{M}] + h_n[\tilde{\mathbf{W}} \otimes \mathbf{I}_{n_{\text{dof}}}]\mathbf{K}(\mathbf{x}_q) \qquad (98)$$

where the matrix $\mathbf{K}(\mathbf{x}_q)$ has the following block structure

$$\mathbf{K}(\mathbf{x}_q) = \nabla_{\mathbf{x}_q}\mathbf{f}(\mathbf{x}_q) = \begin{bmatrix} \mathbf{K}_2(\xi_1)w_1 & \dots & \mathbf{K}_{k+1}(\xi_1)w_1 \\ \vdots & & \vdots \\ \mathbf{K}_2(\xi_k)w_k & \dots & \mathbf{K}_{k+1}(\xi_k)w_k \end{bmatrix} \quad (99)$$

The unknown coordinates for the first iteration within every time step are determined in the physically motivated prestep

$$\mathbf{x}_q^{(0)} = -\mathbf{A}_q^q \otimes \mathbf{q}_1 - h_n \mathbf{A}_p^q \otimes [\mathbb{M}^{-1}\mathbf{p}_1] \quad (100)$$

with

$$\begin{aligned} \mathbf{A}_q^q &= -\mathbf{e}_k \\ \mathbf{A}_p^q &= [\mathbf{A}'']^{-1}\mathbf{A}'[\mathbf{A}'']^{-1}\mathbf{b}'' - [\mathbf{A}'']^{-1}\mathbf{b}' \\ \mathbf{e}_k &= (1,\dots,1) \in \mathbb{R}^k \end{aligned} \quad (101)$$

which initiate the variables by the rigid body motion. The momenta $\mathbf{x}_p$ can be computed subsequently using the now known coordinates $\mathbf{q}_A$, $A = 1,\dots,k+1$:

$$\mathbf{x}_p = \frac{1}{h_n}[\mathbf{A}_m^p \otimes \mathbb{M}]\mathbf{x}_q + \frac{1}{h_n}\mathbf{A}_q^p \otimes [\mathbb{M}\mathbf{q}_1] - \mathbf{A}_p^p \otimes \mathbf{p}_1 \quad (102)$$

with

$$\mathbf{A}_m^p = [\mathbf{A}']^{-1}\mathbf{A}'' \quad \mathbf{A}_q^p = [\mathbf{A}']^{-1}\mathbf{b}'' \quad \mathbf{A}_p^p = [\mathbf{A}']^{-1}\mathbf{b}' \quad (103)$$

As the stopping criterion for the iterative solution procedure, we check in this paper simply the Euclidean norm of the residuum. The vector $\mathbf{x}_q^{(i)}$ is accepted as approximate solution if the norm of the residuum fulfils a tolerance ε in the way

$$\|\mathbf{R}(\mathbf{x}_q^{(i)})\| \le \varepsilon \quad (104)$$

For all simulations, we have chosen a tolerance of $\varepsilon = 10^{-8}$. Note that there are more appropriate stopping criteria necessary for systems with internal variables and thermo-mechanical couplings (see [12]).

Appendix 4: The tangent matrix

The blocks $\mathbf{K}_J$, $J = 2,\dots,k+1$ of the tangent $\mathbf{K}(\mathbf{x}_q)$ in Eq. (99) themselves have again a block structure, given by

$$\mathbf{K}_J = \overset{n_{el}}{\underset{e=1}{\mathbf{A}}} \begin{bmatrix} {}^e\mathbf{K}_J^{11} & \dots & {}^e\mathbf{K}_J^{1n_{en}} \\ \vdots & & \vdots \\ {}^e\mathbf{K}_J^{n_{en}1} & \dots & {}^e\mathbf{K}_J^{n_{en}n_{en}} \end{bmatrix} \quad (105)$$

The blocks ${}^e\mathbf{K}_J^{ab} \in \mathbb{R}^{n_{\dim} \times n_{\dim}}$ can be divided additively in both a geometrical and a material part such that

$${}^e\mathbf{K}_J^{ab} = {}^e\mathbf{K}_{\text{Geo}\,J}^{ab} + {}^e\mathbf{K}_{\text{Mat}\,J}^{ab} \quad (106)$$

Defining for a compact presentation of the tangent matrices the abbreviations

$$\mathbf{B}_a^e = \mathbf{F}_e \otimes \nabla_\eta N_a \cdot \mathbf{J}_e^{-1} \quad (107)$$

$$[{}^e\mathbf{B}_J^b]^T = \mathbf{J}_e^{-T} \cdot \nabla_\eta N_b \otimes [\mathbf{F}_J^e]^T \quad (108)$$

the geometrical and the material parts associated with the cG method read

$${}^e\mathbf{K}_{\text{Geo}\,J}^{ab} = M_J \hat{Q}_{ab}^e \mathbf{I}_{n_{\dim}} \quad (109)$$

$${}^e\mathbf{K}_{\text{Mat}\,J}^{ab} = M_J \int_{\mathscr{B}_0^e} \mathbf{B}_a^e : \mathscr{L}(\mathbf{C}_e,\mathbf{A}) : [\mathbf{B}_b^e]^T \mathrm{d}V \quad (110)$$

For the eG method, especially the material parts of the tangent operator are more complicated due to the additional terms of the enhanced gradient:

$${}^e\underline{\mathbf{K}}_{\text{Geo}\,J}^{ab} = M_J \underline{\mathsf{Q}}_{ab}^e \mathbf{I}_{n_{\dim}}$$

$${}^e\underline{\mathbf{K}}_{\text{Mat}\,J}^{ab} = \int_{\mathscr{B}_0^e} \mathbf{B}_a^e : \left[M_J \mathscr{L}(\mathbf{C}_e,\mathbf{A}) + 4M_J' \frac{\mathscr{G}_e}{\underline{\mathscr{N}}_e}\mathbb{I} \right] : [{}^e\mathbf{B}_J^b]^T \mathrm{d}V$$

$$+ \int_{\mathscr{B}_0^e} \mathbf{B}_a^e : \left[\frac{2\delta_{J,k+1}}{\underline{\mathscr{N}}_e} \frac{\partial \mathbf{C}_e}{\partial \alpha} \otimes \mathbf{S}_J^e \right.$$

$$\left. - \frac{4}{\underline{\mathscr{N}}_e} \frac{\partial \mathbf{C}_e}{\partial \alpha} \otimes \underline{\mathsf{L}}_1^e \right] : [{}^e\mathbf{B}_J^b]^T \mathrm{d}V$$

$$- \int_{\mathscr{B}_0^e} \mathbf{B}_a^e : \left[\frac{4\underline{\mathscr{G}}}{\underline{\mathscr{N}}_e^2} \frac{\partial \mathbf{C}_e}{\partial \alpha} \otimes {}^e\underline{\mathsf{L}}_2^b \right] \mathrm{d}V$$

where

$$\underline{\mathsf{L}}_1^e = \sum_{l=1}^k \left\{ M_J(\xi_l) \frac{\partial \mathbf{C}_e(\xi_l)}{\partial \alpha} : \nabla_{\mathbf{C}_e}^2 W_e(\mathbf{C}_e(\xi_l),\mathbf{A}) \right.$$

$$\left. + M_J'(\xi_l) \left[\nabla_{\mathbf{C}_e} W_e(\mathbf{C}_e(\xi_l),\mathbf{A}) + \frac{\mathscr{G}_e}{\underline{\mathscr{N}}_e} \frac{\partial \mathbf{C}_e(\xi_l)}{\partial \alpha} \right] \right\} w_l$$

$${}^e\underline{\mathsf{L}}_2^b = \sum_{l=1}^k \frac{\partial \mathbf{C}_e(\xi_l)}{\partial \alpha} : \left\{ M_J'(\xi_l)[\mathbf{B}_b^e(\xi_l)]^T \right.$$

$$\left. + M_J(\xi_l) \left[\frac{\partial \mathbf{B}_b^e(\xi_l)}{\partial \alpha} \right]^T \right\} w_l$$

Note that these tangent matrices only apply for the case that the vector of the non-conservative forces $\mathbf{f}_{nc}$ does not depend on the coordinates $\mathbf{q}$ and the momenta $\mathbf{p}$, respectively.

Appendix 5: The material tangent operator

The material tangent operator $\mathscr{L}$, see Reference [18], necessary in the linearisation of the semi-discrete equations of motion, is a fourth-order tensor resulting from the gradient of the second PIOLA–KIRCHHOFF stress tensor. Defining the short hand notations

$$\mathbb{I}_{ijkl} = \frac{1}{2}(\delta_{ik}\delta_{jl} + \delta_{il}\delta_{jk}) \tag{111}$$

$$\left\{(\mathbf{A} \otimes \mathbf{I})^{S24}\right\}_{ijkl} = \frac{1}{4}(A_{il}\delta_{jk} + A_{jl}\delta_{ik} + A_{ik}\delta_{jl} + A_{jk}\delta_{il}) \tag{112}$$

$$\left\{-\mathbf{C}^{-1} \odot \mathbf{C}^{-1}\right\}_{ijkl} = -\frac{1}{2}(C_{ik}^{-1}C_{lj}^{-1} + C_{il}^{-1}C_{kj}^{-1}) \tag{113}$$

of the symmetric fourth-order unity tensor $\mathbb{I}$, the minor and major symmetric product $(\mathbf{A} \otimes \mathbf{I})^{S24}$ of the structural tensor $\mathbf{A}$ with the unity tensor $\mathbf{I}$ and the major symmetric product $\odot$ of the symmetric inverse right CAUCHY–GREEN tensor, this fourth-order tensor takes the form (cf. [16] and [24])

$$\mathscr{L}(\mathbf{C}, \mathbf{A}) = 2\nabla_{\mathbf{C}}\mathbf{S} = 4\nabla_{\mathbf{C}}^2 W$$

$$= 4\sum_{i=1}^{5}\left\{\frac{\partial I_i}{\partial \mathbf{C}} \otimes \left[\sum_{j=1}^{5}\frac{\partial}{\partial I_j}\left(\frac{\partial W}{\partial I_i}\right)\frac{\partial I_j}{\partial \mathbf{C}}\right]\right.$$
$$\left. + \frac{\partial W}{\partial I_i}\frac{\partial}{\partial \mathbf{C}}\left(\frac{\partial I_i}{\partial \mathbf{C}}\right)\right\}$$

$$= \left\{\frac{\partial^2 W}{\partial I_1^2} + 2I_1\frac{\partial^2 W}{\partial I_1 \partial I_2} + \frac{\partial W}{\partial I_2} + I_1^2\frac{\partial^2 W}{\partial^2 I_2}\right)\mathbf{I} \otimes \mathbf{I}$$

$$- \left(\frac{\partial^2 W}{\partial I_1 \partial I_2} + I_1\frac{\partial^2 W}{\partial^2 I_2}\right)(\mathbf{C} \otimes \mathbf{I} + \mathbf{I} \otimes \mathbf{C}) + \frac{\partial^2 W}{\partial^2 I_2}\mathbf{C} \otimes \mathbf{C}$$

$$- \frac{\partial W}{\partial I_2}\mathbb{I} + \left(\frac{\partial^2 W}{\partial I_1 \partial I_4} + I_1\frac{\partial^2 W}{\partial I_2 \partial I_4}\right)(\mathbf{A} \otimes \mathbf{I} + \mathbf{I} \otimes \mathbf{A})$$

$$- \frac{\partial^2 W}{\partial I_2 \partial I_4}(\mathbf{C} \otimes \mathbf{A} + \mathbf{A} \otimes \mathbf{C}) + \frac{\partial^2 W}{\partial I_4 \partial I_4}\mathbf{A} \otimes \mathbf{A}$$

$$+ \left(\frac{\partial^2 W}{\partial I_1 \partial I_5} + I_1\frac{\partial^2 W}{\partial I_2 \partial I_5}\right)[\mathbf{I} \otimes (\mathbf{AC} + \mathbf{CA})$$
$$+ (\mathbf{AC} + \mathbf{CA}) \otimes \mathbf{I}]$$

$$- \frac{\partial^2 W}{\partial I_2 \partial I_5}[(\mathbf{C} \otimes (\mathbf{AC} + \mathbf{CA}) + (\mathbf{AC} + \mathbf{CA}) \otimes \mathbf{C}]$$

$$+ \frac{\partial^2 W}{\partial I_5 \partial I_5}[(\mathbf{AC} + \mathbf{CA}) \otimes (\mathbf{AC} + \mathbf{CA})]$$

$$+ \frac{\partial W}{\partial I_4 \partial I_5}[(\mathbf{A} \otimes (\mathbf{AC} + \mathbf{CA}) + (\mathbf{AC} + \mathbf{CA}) \otimes \mathbf{A}]$$

$$+ \frac{\partial W}{\partial I_5}(\mathbf{A} \otimes \mathbf{I})^{S24} + I_3\left(I_3\frac{\partial^2 W}{\partial I_3 \partial I_3} + \frac{\partial W}{\partial I_3}\right)\mathbf{C}^{-1} \otimes \mathbf{C}^{-1}$$

$$+ I_3\frac{\partial W}{\partial I_3}(-\mathbf{C}^{-1} \odot \mathbf{C}^{-1})$$

$$+ I_3\left(\frac{\partial^2 W}{\partial I_1 \partial I_3} + I_1\frac{\partial^2 W}{\partial I_2 \partial I_3}\right)(\mathbf{I} \otimes \mathbf{C}^{-1} + \mathbf{C}^{-1} \otimes \mathbf{I})$$

$$- I_3\frac{\partial^2 W}{\partial I_2 \partial I_3}(\mathbf{C} \otimes \mathbf{C}^{-1} + \mathbf{C}^{-1} \otimes \mathbf{C})$$

$$+ I_3\frac{\partial^2 W}{\partial I_3 \partial I_4}(\mathbf{A} \otimes \mathbf{C}^{-1} + \mathbf{C}^{-1} \otimes \mathbf{A})$$

$$+ I_3\frac{\partial^2 W}{\partial I_3 \partial I_5}[(\mathbf{AC} + \mathbf{CA}) \otimes \mathbf{C}^{-1} + \mathbf{C}^{-1} \otimes (\mathbf{AC} + \mathbf{CA})] \tag{114}$$

Note that Eq. (114) also represents the universal case, and does not require a split of the free energy density function into an isochoric and volumetric part.

References

1. Groß M (2004) Conserving time integrators for nonlinear elastodynamics. Ph.D. Dissertation, University of Kaiserslautern
2. Groß M, Betsch P, Steinmann P (2005) Conservation properties of a time FE method. Part IV: higher order energy and momentum conserving schemes. Int J Numer Methods Eng 63:1849–1897
3. Betsch P, Steinmann P (2000) Conservation properties of a time FE method. Part I: time-stepping schemes for N-body problems. Int J Numer Methods Eng 49:599–638
4. Betsch P, Steinmann P (2001) Conservation properties of a time FE method. Part II: time-stepping schemes for nonlinear elastodynamics. Int J Numer Methods Eng 50:1931–1955
5. Simo JC, Tarnow N, Wong KK (1992) Exact energy-momentum conserving algorithms and symplectic schemes for nonlinear dynamics. Comput Methods Appl Mech Eng 100:63–116
6. Betsch P, Steinmann P (2000) Inherently energy conserving time finite elements for classical mechanics. J Comput Phys 160:88–116
7. Eriksson K, Estep D, Hansbo P, Johnson C (1996) Computational differential equations. Cambridge University Press, Cambridge
8. Hulme BL (1972) Discrete Galerkin and related one-step methods for ordinary differential equations. Math Comput 26(120):881–891
9. Hulme BL (1972) One-step piecewise polynomial Galerkin methods for initial value problems. Math Comput 26(118):415–426
10. Gonzalez O, Simo JC (1996) On the stability of symplectic and energy-momentum algorithms for nonlinear Hamiltonian systems with symmetry. Comput Methods Appl Mech Eng 134:197–222
11. Simo JC, Tarnow N (1992) The discrete energy-momentum method. Conserving algorithms for nonlinear elastodynamics. Zeitschrift fur Angewandte Mathematik und Physik 43:757–792
12. Groß M (2009) Higher-order accurate and energy-momentum consistent discretisation of dynamic finite deformation thermo-viscoelasticity. Habilitation thesis, University of Siegen
13. Gonzalez O (1996) Design and analysis of conserving integrators for nonlinear Hamiltonian systems with symmetry. Ph.D. Dissertation, Stanford University, Stanford, CA
14. Gonzalez O (2000) Exact energy and momentum conserving algorithms for general models in nonlinear elasticity. Comput Methods Appl Mech Eng 190:1763–1783
15. Müller M, Groß M, Betsch P (2008) Material models in principal stretches for elastodynamics. Proc Appl Math Mech (PAMM) 8:10315–10316. doi:10.1002/pamm.200810315
16. Holzapfel GA (2000) Nonlinear solid mechanics. Wiley, London
17. Menzel A (2002) Modelling and computation of geometrically nonlinear anisotropic inelasticity. Ph.D. Dissertation, University of Kaiserslautern
18. Schröder J, Neff P (2010) Poly-, quasi- and rank-one convexity in applied mechanics. CISM courses and lectures, vol 516, Springer, New York

19. Spencer AJM (1971) Theory of invariants. In: Eringen AC (ed) Continuum physics, vol 1. Academic Press, New York
20. Betten J (1987) Formulation of anisotropic constitutive equations. In: Boehler JP (ed) Applications of tensor functions in solid mechanics CISM Course No. 292. Springer, New York
21. Boehler JP (1987) Introduction to the invariant formulation of anisotropic constitutive equations. In: Boehler JP (ed) Applications of tensor functions in solid mechanics CISM course No. 292. Springer, New York
22. Zheng QS, Spencer AJM (1993) Tensors which characterize anisotropies. Int J Eng Sci 31:679–693
23. Ball JM (1977) Convexity conditions and existence theorems in non-linear elasticity. Arch Rat Mech Anal 63:337–403
24. Schröder J, Neff P (2003) Invariant formulation of hyperelastic transverse isotropy based on polyconvex free energy functions. Int J Solid Struct 40:401–445
25. Ebbing V, Schroeder J, Neff P, Gruttmann F (2009) Micromechanical modeling of woven fiber composites for the construction of effective anisotropic polyconvex energies. Proc Appl Math Mech 9:333–334
26. Holzapfel GA (2000) Biomechanics of Soft Tissue. Biomech Preprint Series
27. Itskov M, Ehret AE (2009) A universal model for the elastic, inelastic and active behaviour of soft biological tissues. GAMM-Mitt 32(2):221–236
28. Kern D, Bär S, Groß M (2014) Variational Integrators for thermomechanical coupled dynamic systems with heat conduction. Proc Appl Math Mech (PAMM) 14:47–48. doi:10.1002/pamm.201410016
29. Kaliske M (2000) A formulation of elasticity and viscoelasticity for fibre reinforced material at small and finite strains. Comput Methods Appl Mech Eng 185:225–243
30. Holzapfel GA, Gasser TC (2001) A viscoelastic model for fiber-reinforced composites at finite strains: continuum basis, computational aspects and applications. Comput Methods Appl Mech Eng 190:4379–4403
31. Truesdell C, Noll W (2004) The non-linear field theories of mechanics. Springer, New York
32. Wriggers P (2008) Nonlinear finite element methods. Springer, Berlin
33. Hartmann S, Neff P (2003) Polyconvexity of generalized polynomial-type hyperelastic strain energy functions for near-incompressibility. Int J Sol Struc 40:2767–2791
34. Schröder J, Neff P, Balzani D (2005) A variational approach for materially stable anisotropic hyperelasticity. Int J Solid Struct 42:4352–4371
35. Groß M, Betsch P (2011) Galerkin-based energy-momentum consistent time-stepping algorithms for classical nonlinear thermo-elastodynamics. Math Comput Simul 82:718–770
36. Soutis C (2005) Carbon fiber reinforced plastics in aircraft construction. Mater Sci Eng A 412:171–176
37. Romero I (2010) Algorithms for coupled problems that preserve symmetries and the laws of thermodynamics. PartI: monolithic integrators and their application to finite strain thermoelasticity. Comput Methods Appl Mech Eng 199:1841–1858
38. Schröder J, Neff P (2002) Application of Polyconvex Anisotropic Free Energies to Soft Tissues. H.A. Mang, F.G. Rammersdorfer and J. Eberhardsteiner, editors, Proceedings of 5th World Congress on Computational Mechanics (WCCM V), Vienna, Austria, 7–12 July 2002